The anharmonic force field and equilibrium molecular structure of ketene

Allan L. L. East and Wesley D. Allen
Department of Chemistry, Stanford University, Stanford, California 94305

Stephen J. Klippenstein
Department of Chemistry, Case Western Reserve University, Cleveland, Ohio 44106

(Received 8 July 1994; accepted 16 November 1994)

A comprehensive anharmonic vibrational analysis of isotopic ketenes has been performed on the basis of a complete *ab initio* quartic force field constructed by means of second-order Møller–Plesset perturbation theory (MP2) and the coupled-cluster singles and doubles (CCSD) approach, augmented for structural optimizations by a contribution for connected triple excitations [CCSD(T)]. The atomic-orbital basis sets of the study entailed C,O$(10s6p/5s4p)$ and H$(6s/4s)$ spaces multiply polarized in the valence region to give QZ$(2d,2p)$ and QZ$(2d1f,2p1d)$ sets. An iterative *anharmonic* vibrational refinement of a limited set of quadratic scaling parameters on 27 fundamentals of H_2CCO, HDCCO, D_2CCO, and $H_2C^{13}CO$ generates a final quartic force field which reproduces the empirical ν_i data with an average absolute error of only 1.1 cm^{-1}. This force field yields a complete and self-consistent set of Coriolis (ζ_{ij}), vibrational anharmonic (χ_{ij}), vibration–rotation interaction (α_i), and quartic and sextic centrifugal distortion constants, providing a critical assessment of the assorted spectroscopic constants determined over many years and also facilitating future computations of vibrational state densities for detailed tests of unimolecular dissociation theories. The harmonic frequencies ascertained for H_2CCO (in cm^{-1}), with associated anharmonicities in parentheses, are $\omega_1(a_1)=3202.2(-129.2)$, $\omega_2(a_1)=2197.2(-44.4)$, $\omega_3(a_1)=1415.2(-25.9)$, $\omega_4(a_1)=1146.0(-29.7)$, $\omega_5(b_1)=581.9(+7.1)$, $\omega_6(b_1)=502.6(+26.3)$, $\omega_7(b_2)=3308.2(-141.3)$, $\omega_8(b_2)=996.0(-17.9)$, and $\omega_9(b_2)=433.6(+5.0)$. The large positive anharmonicity for the $\nu_6(b_1)$ C═C═O bending mode, which is principally a Coriolis effect, warrants continued investigation. Explicit first-order treatments of the strong Fermi interactions within the $(\nu_4,2\nu_5,\nu_5+\nu_6,2\nu_6)$ manifold reveal resonance shifts for ν_4(H_2CCO, HDCCO, D_2CCO) of $(-12.1, -10.0, +12.2)$ cm^{-1}, in order. The experimental assignments for this Fermi tetrad are confirmed to be problematic. From high-precision empirical rotational constants of six isotopomers and the theoretical anharmonic force field, the equilibrium structure of ketene is derived: r_e(C═O)=1.160 30(29) Å, r_e(C═C)=1.312 12(30) Å, r_e(C–H)=1.075 76(7) Å, and θ_e(H–C–H)=121.781(12)°. A natural bond orbital (NBO) analysis shows that the unusually large methylene angle is attributable to extensive in-plane π delocalization. © *1995 American Institute of Physics.*

I. INTRODUCTION

The rich history[1–33] of infrared and microwave studies of the ketene molecule is a microcosm of the development of modern spectroscopy over the last six decades. Infrared bands of gaseous ketene were reported in a communication from Harvard in 1937,[2] following publication of the liquid Raman spectrum in the German literature the previous year.[1] In the immediate postwar period, this semirigid, near-prolate asymmetric rotor, whose dipole moment is sizeable, was identified in the 20 GHz region, and thus the rotational spectrum of ketene became an early target of burgeoning microwave techniques, owing to the contemporaneous rationale[9] that ''its spectrum is difficult enough to be interesting but perhaps simple enough to be precisely analyzed.'' In a series of microwave studies,[6,7,9,14] ground-state rotational constants of five isotopic ketenes were accumulated and employed in r_s structure determinations, while the relative intensities of satellite bands were analyzed to estimate the positions of low-frequency bending fundamentals. Simultaneous infrared work on gaseous ketene[3–5,10–13] and its deuterated variants,[8,11,12] which achieved partial resolution of rotational band contours, augmented the microwave data on the molecular structure, established most of the isotopomeric set of vibrational fundamentals, and provided tentative assignments for numerous overtone and combinations levels, many of which have yet to be confirmed or reanalyzed in high resolution. Nonetheless, a bewildering set of conflicting assignments and alternate normal coordinate analyses[3,12,15] resulted for the perpendicular bands in the 400–1000 cm^{-1} region, a direct manifestation of the unusual spectral complexity present.

The enigma of the low-frequency bending modes was resolved in 1963. Refined microwave relative intensity measurements[16] implicated a fundamental lying nearly 100 cm^{-1} lower than any previous assignment, and concurrent matrix-isolation infrared spectroscopy[17] provided definitive evidence for this interpretation. In particular, the pioneering argon-matrix experiments of Moore and Pimentel,[17] complemented by solid phase spectra, revealed $\nu_9(b_2)=438$, 398, and 371 cm^{-1}, in order, for ketene-h_2, -d_1, and -d_2, while the 750–950 cm^{-1} interval proved devoid of IR-active fundamental absorptions previously ascribed to this region. With additional gas-phase data and correct vibrational assignments

 0021-9606/95/102(21)/8506/27/$6.00

at hand, a quadratic force field was derived, quartic centrifugal distortion and Coriolis parameters were predicted, and new hydrogen position coordinates were ascertained from a-axis inertial moments.[17] The sesquidecade following 1963 brought a progressive buildup of spectroscopic information on ketene. The hybrid orbital force field method was applied,[18] the issue of discrimination between alternate solutions in force field refinements was surveyed,[19] the B-type perpendicular infrared bands in the $(\nu_7,\nu_2+\nu_8)$ manifold near 3150 cm^{-1} were analyzed under high resolution to obtain reliable data on A_0 and D_K,[20] numerous new lines were observed in the millimeter-wave region up to 220 GHz,[20,21] and the set of centrifugal distortion parameters was improved and extended to sextic terms.[20,21] These accomplishments lead to an updated force field[22] containing 16 of the 19 possible quadratic elements, from which an r_z structure was determined and Coriolis parameters as well as Δ_J, Δ_K, Δ_{JK}, δ_J, and δ_K distortion constants were recomputed.

Because ketene is a highly reactive and extremely poisonous substance, boiling near -50 °C and prone to dimerization, some of the early spectroscopic efforts[3,10,11] were hindered by impurities, particularly ethylene, carbon dioxide, acetylene, and diketene. While improvements in synthesis and handling techniques have largely circumvented this problem, the inherent complexity of the rovibrational spectrum has been a persistent obstacle, rendering detailed analyses much more elusive than first envisioned. A very recent characterization[33] of the quagmire encountered over the years is apt: ''[Many] vibrational bands of this molecule suffer severe perturbations, mainly because of the presence of relatively low-lying vibrational states (ν_5=587 cm^{-1}, ν_6=528 cm^{-1}, ν_9=439 cm^{-1}), whose overtone and combination bands are scattered all over the mid-infrared region and give rise to Fermi and Coriolis interactions, in addition to localized level crossings, that distort the rotational structure of the bands.'' Such intricate phenomena have sustained interest in the rovibrational spectrum of ketene during the last two decades.

In 1978, Nemes[23] employed a simplified model Hamiltonian to deperturb the interacting K manifolds of the $(\nu_9,\nu_6,\nu_5,\nu_8)$ tetrad, which exhibit strong Coriolis resonances effected by a-axis molecular rotations. These Coriolis interactions were later probed and analyzed in successively greater detail by Hegelund *et al.*,[24,30] who tabulated myriad lines within the ν_9, ν_6, ν_5, $2\nu_9-\nu_9$, $\nu_9+\nu_6-\nu_9$, $2\nu_6-\nu_6$, and $\nu_4-\nu_6$ bands of D_2CCO and extracted the molecular constants in the ground-state rotational Hamiltonian of this isotopomer with extreme precision. Shortly thereafter, all fundamental bands except ν_9, as well as the overtones $2\nu_5$, $2\nu_6$, and $2\nu_8$, of both ketene and its ^{13}C isotopic derivatives were reinvestigated by high-resolution infrared techniques for the first time, the four a_1 fundamentals of D_2CCO also being revisited.[26,27] These 1987 studies by Duncan and collaborators[26,27] encountered pervasive Fermi resonance interactions, particularly acute within the $(\nu_3,\nu_8+\nu_9)$ and $(\nu_4,2\nu_5,2\nu_6,\nu_5+\nu_6)$ manifolds, which in many cases produced irregular subband origins and bizarre isotopic frequency shifts. A telling quote[27] summarizes the situation: ''On account of the wide spread of individual bands in the gas phase spectrum, arising principally from the very large A rotational constant, the possibility of perturbations within the bands was anticipated. Nevertheless, we were not prepared for the apparent complexity of perturbation which we have found.''

In order to assimilate the spectroscopic data from the 1987 studies, a critical assessment of all available information for ketene and deuterated variants was subsequently executed.[28] Notably, the collection of fundamental band origins and ^{13}C frequency shifts was scrutinized for perturbation anomalies and approximately corrected for anharmonicity, and incompatibilities and truncation effects among infrared/microwave sets of quartic centrifugal distortion constants were exposed. This groundwork facilitated the refinement[28] of a comprehensive general harmonic force field (GHFF) in which constraints on small, indeterminate quadratic interaction constants were based on restricted Hartree–Fock (RHF) *ab initio* predictions. A revised r_z structure and estimated r_e parameters were subsequently derived from the GHFF.[29] Despite limitations in the underlying spectroscopic data set, this force field provides the most realistic harmonic potential function currently available.

In recent years there has been renewed interest in the pure rotational states of isotopic ketenes, interrogated not only with microwave techniques[25,31,33] but also via Raman spectroscopy,[32] which until 1990 had not been applied to ketene since 1936.[1] The number of catalogued IR and microwave ground-state combination differences is now well over 2000, and these data appear to determine even some of the sextic and octic distortion parameters with some precision. The 1990 microwave study of Brown *et al.*[31] produced the first microwave measurements of $H_2C^{13}CO$ lines and supplanted the outdated 1959 data[14] for $H_2{}^{13}CCO$ and $H_2CC^{18}O$, thus completing the determination of high-precision rotational constants for monosubstituted isotopic ketenes. The resulting collection of empirical (A_0,B_0,C_0) constants establishes the r_0 and r_s structures of ketene,[31] as well as approximate (r_m^{ρ}) equilibrium parameters,[31] and comprises the foundation for a rigorous r_e structural refinement based on high-quality theoretical vibration–rotation interaction constants.

Further extension of the historical progression of efforts to catalog and assign the rovibrational energy levels of ketene and account for them with a comprehensive molecular Hamiltonian is predicated on the determination of a valid anharmonic force field, particularly to assist in the deperturbation of Fermi and Coriolis resonances and in the interpretation of enigmatic band structures. Therefore, in this article a complete quartic force field is determined by means of correlated *ab initio* methods and subjected to a well-based and limited refinement in order to reproduce all observed fundamental vibrational frequencies of ketene isotopomers to within a few cm^{-1}. The iterative vibrational procedure, which explicitly treats major Fermi resonances in first order, yields for the first time a complete and self-consistent set of vibrational anharmonic (χ_{ij}), vibration–rotation interaction (α_i), quartic and sextic centrifugal distortion, and Coriolis constants, in addition to harmonic vibrational frequencies (ω_i) and a precisely determined r_e structure.

An overriding enticement for pursuing an extensive anharmonic vibrational analysis of ketene is afforded by the numerous experiments[34–45] within the last decade which have probed the photofragmentation dynamics of this molecule in unprecedented detail, testing the very foundations of contemporary theories of unimolecular dissociation. Photoexcitation of ketene to the S_1 state ($\tilde{A}\ ^1A''$) is promptly followed either by intersystem crossing to $T_1(\tilde{a}\ ^3A'')$, which correlates to $CH_2(\tilde{X}\ ^3B_1)+CO$ via in-plane bent structures, or by internal conversion to S_0, which yields $CH_2(\tilde{a}\ ^1A_1)+CO$ along out-of-plane bent paths.[37,40,42,43] Several experimental investigations have quantified the dissociation rate of ketene at selected energies ranging from near the triplet threshold (28 296 cm^{-1})[40] to 5600 cm^{-1} in excess of the singlet threshold (30 116 cm^{-1}).[37,39] Moreover, singlet/triplet branching ratios have been ascertained up to 2500 cm^{-1} above the singlet onset,[42] providing individual, state-specific rate constants for both the S_0 and T_1 channels.

Dissociation on the triplet surface proceeds over a small, 3.8 kcal mol^{-1} barrier,[40] rendering the fragmentation dynamics essentially impulsive and causing carbon monoxide to be rotationally hot in the product state energy distributions.[41] The observation[45] of stepwise increases in the rate of dissociation of triplet ketene has provided dramatic evidence of quantized transition-state vibrational thresholds, a fundamental premise of RRKM theory.[46,47] Complementary in nature to the triplet fragmentation is the dissociation on the S_0 surface of ketene, which has been established as one of the most completely and accurately characterized barrierless reactions,[34,36–39,43,44,57] thus stimulating the development of improved statistical models for treating loose dynamical bottlenecks by means of microcanonical variational transition state theory.[48–57] Photofragment excitation (PHOFEX) spectra have revealed singlet product state rotational distributions which are highly statistical, in accord with simple phase space theory (PST), although the associated vibrational excitation probabilities are not similarly reproduced.[34,37,38,43,44] Account for all observed experimental data for the singlet fragmentation channel appears to be provided by a variational RRKM model[48–55,57] implementing the hybrid dynamical assumptions of Marcus,[49] wherein the number of available states for dissociation is determined as a convolution of a direct quantum count for conserved modes and a Monte Carlo evaluation of corresponding classical phase space volumes for transitional modes. Both the location and the form of the hypersurface separating reactants and products prove to be important,[52–55,57] as well as the joint incorporation of inner and outer variational transition states acting in series.[57] The crux is that such models cannot be quantitatively applied without improved calculations for the density of highly excited reactant vibrational states, a task facilitated by the anharmonic vibrational analysis detailed in this article.

II. THEORETICAL METHODS

Electronic energies of ground-state ketene were determined in this investigation by means of three electron-correlation procedures, viz., the coupled-cluster singles and doubles method (CCSD),[58–63] second-order Møller–Plesset perturbation theory (MP2),[64–67] and CCSD theory augmented by a quasiperturbative term arising from connected triple excitations [CCSD(T)].[68,69] In each instance the reference electronic wave functions were constructed from single-configuration, restricted Hartree–Fock (RHF) molecular orbitals.[66,67,70] The $1s$ core orbitals of the carbon and oxygen atoms were frozen in the correlation treatments as well as the associated core-localized virtual orbitals appearing above 20 a.u., thus excluding a total of 6 orbitals from the active space in all procedures. The electronic structure computations were performed with the program packages PSI[71] and GAUSSIAN92.[72]

Two atomic-orbital basis sets denoted as QZ$(2d,2p)$ and QZ$(2d1f,2p1d)$ were employed here. For these sets the leading designation QZ is *broadly* descriptive of the valence sp space, and the suffixes in parentheses specify the number and types of polarization manifolds appended to the (C,O) and H atoms, in order. For carbon and oxygen, the QZ sp basis consists of the $(10s6p)$ Gaussian primitives of Huzinaga[73] and the $(5s4p)$ contractions of Dunning.[74] As such, these sets are not fully quadruple-ζ in quality—the QZ designation is used primarily to distinguish them from the alternate $(5s3p)$ contractions.[74] The QZ hydrogen basis is a $(6s/4s)$ set constructed from unscaled Huzinaga primitives[73] according to the contractions tabulated by Allen and Schaefer.[75] The orbital exponents of the polarization manifolds are the correlation-optimized values of Dunning,[76] specifically, $\alpha_d(C)=(0.318,\ 1.097)$, $\alpha_f(C)=0.761$, $\alpha_d(O)=(0.645,\ 2.314)$, $\alpha_f(O)=1.428$, $\alpha_p(H)=(0.388,\ 1.407)$, and $\alpha_d(H)=1.057$. Generally, the d and f sets were implemented only with real combinations of the $l=2$ and $l=3$ spherical harmonics, giving a total of 101 and 132 contracted Gaussian functions, respectively, for the QZ$(2d,2p)$ and QZ$(2d1f,2p1d)$ basis sets. However, in the QZ$(2d,2p)$ MP2 computations of higher-order force constants, the supernumerary Cartesian d orbitals were not excluded from the one-particle basis.

Analytic gradient techniques for the CCSD[63,77] and CCSD(T)[78] methods were utilized in the optimization of geometric structures to 10^{-6} Å or rad in the internal coordinate space. Equilibrium parameters at the QZ$(2d,2p)$ CCSD and QZ$(2d1f,2p1d)$ CCSD(T) levels of theory are reported in Table I. Selected total energies[79] at these structures are QZ$(2d,2p)$ RHF$(-151.784\,454)$ and CCSD$(-152.299\,160)$//QZ$(2d,2p)$ CCSD; QZ$(2d,2p)$ RHF$(-151.783\,560)$, MP2$(-152.293\,222)$, and CCSD$(-152.299\,067)$//QZ$(2d1f,2p1d)$ CCSD(T); and QZ$(2d1f,2p1d)$ RHF$(-151.789\,086)$, CCSD$(-152.343\,744)$, and CCSD(T)$(-152.370\,747)$ //QZ$(2d1f,2p1d)$ CCSD(T). The Euclidean norm of the t_1 amplitudes is near 0.017 in the various CCSD results, a diagnostic[80] indicating only a modest degree of multireference character in the ground-state electronic wave function. The equilibrium dipole moments μ_e[QZ$(2d,2p)$ CCSD] $=-1.3391$ D and μ_e[QZ$(2d1f,2p1d)$ CCSD(T)]$=-1.3387$ D are computed as energy derivatives with respect to an external electric field, in very good agreement with the observed microwave value $\mu_0=1.414$ D for the ground vibrational state.[9]

TABLE I. Geometric structures of ketene.[a]

	r(C=O)	r(C=C)	r(C–H)	θ(H–C–H)
Ab initio equilibrium data				
DZP CISD[b]	1.166 9	1.319 5	1.078 5	121.83
QZ($2d,2p$) CCSD	1.159 7	1.315 5	1.075 8	121.97
QZ($2d1f,2p1d$) CCSD(T)	1.165 8	1.318 9	1.078 2	121.89
Spectroscopic parameters[c]				
r_0 (a, 1990)	1.162 6 (57)	1.314 7 (60)	1.090 5 (18)	123.46 (29)
(c, 1976)	1.161 (2)	1.316 (2)	1.078 0 (10)	122.01 (20)
r_s (a, 1990)	1.162 0(721)	1.313 7(721)	1.082 5 (15)	122.56 (1)
(c, 1976)	1.161 8 (30)	1.315 9 (30)	1.074 0 (18)	122.17 (20)
r_z (b, 1987)	1.161 4 (14)	1.316 5 (15)	1.080 02(33)	121.978(62)
(c, 1976)	1.160 8 (20)	1.317 1 (20)	1.079 7 (10)	121.97 (20)
r_m^{ρ}(a, 1990)	1.160 0 (58)	1.314 0 (62)	1.074 0 (19)	121.58 (29)
Empirically derived r_e structures[d]				
r_e(I; ls-ABC)	1.160 30(29)	1.312 12(30)	1.075 76 (7)	121.781(12)
r_e(II; ls-BC)	1.160 31(20)	1.312 12(21)	1.075 84 (6)	121.789 (9)
r_e(III; Kr-BC, D_2CCO)	1.160 37	1.312 22	1.076 11	121.828
r_e(IV; Kr-BC, HDCCO)	1.160 36	1.312 23	1.076 26	121.833

[a]Bond distances in Å and bond angles in deg. When appropriate, standard errors are given in parentheses in units of the last digit of the associated quantity.

[b]Reference 134.

[c]The labels a, b, and c denote, in order, Refs. 31, 29, and 22, studies from the years 1990, 1987, and 1976, respectively.

[d]In structures I and II, ls-ABC and ls-BC denote least-squares fits to isotopomeric sets of (I_e^A, I_e^B, I_e^C) and (I_e^B, I_e^C) moments of inertia, respectively. Structures III and IV result from Kraitchman analyses applied to (I_e^B, I_e^C) sets with D_2CCO and HDCCO data, respectively, used to locate the hydrogen atoms. The final structure recommended here is r_e(I; ls-ABC).

Quadratic force fields and dipole moment derivatives were evaluated via analytic second-derivative techniques for MP2 wave functions[81,82] and by finite differences of analytic gradients in the CCSD case.[63,77] The complete set of cubic and quartic force constants of ketene was determined at the QZ($2d,2p$) MP2 level from analytic second derivatives computed at 69 structures displaced about an assumed reference geometry. In all numerical differentiation schemes, displacement increments of ± 0.005 Å and ± 0.01 rad were employed for the various internal coordinates. The numerical procedures are described further in Sec. III, where the high precision achieved by the methods is demonstrated. Refinement of the *ab initio* quadratic force constants was accomplished by applying the scaled quantum mechanical (SQM) force field technique[83–89] to sets of harmonic frequencies derived from the empirical fundamentals of ketene isotopomers. A recent paper by Allen *et al.*[89] succinctly presents the formalism of the SQM procedure and reviews previous applications of this method. In the harmonic vibrational analyses, normal modes (Q_i) were quantitatively assigned in internal coordinates by means of the associated total energy distributions (TEDs),[89–91] and integrated infrared band intensities were computed within the double-harmonic approximation[92,93] via the formula $A_i = 42.254\,72\,|\partial\boldsymbol{\mu}/\partial Q_i|^2$, where A_i is in km mol^{-1}, and $(\partial\boldsymbol{\mu}/\partial Q_i)$ is in D Å^{-1} amu$^{-1/2}$.

III. PROCEDURE FOR VIBRATIONAL ANALYSIS

The anharmonic vibrational analysis of the ketene molecule is effectuated here by the application of second-order perturbation theory to the standard vibration–rotation Hamiltonian[94–98] containing a potential energy surface expansion through quartic terms. The use of *ab initio* anharmonic force fields in this approach has been investigated extensively in recent systematic studies of linear and asymmetric top molecules by Allen and co-workers[99–104] and in a large body of work by several other research groups.[105–118] In principle, this methodology is well suited for the semirigid ketene molecule, but particular concern must be given the numerous vibrational resonances exhibited by the parent species and its isotopic variants.

The goal of the present analysis is to obtain a quantitatively accurate anharmonic force field which satisfies two primary criteria: (1) the fundamental frequencies definitively established through high-resolution infrared spectroscopy are reproduced to better than 3 cm^{-1} and (2) the reference geometry for the potential surface expansion and subsequent vibrational treatment is the true r_e structure of ketene, as derived from high-precision microwave rotational constants via the anharmonic vibrational procedure itself. Of the 238 unique constants in the complete quartic force field of ketene, only the quadratic parameters are subjected here to empirical refinement through the use of ten variable scale factors within a generalized SQM formalism. In this way the goals of the analysis are met with only limited modifications of a high-quality *ab initio* force field via a scaling scheme based on firm physical foundations. A flow chart for the vibrational procedure is presented in Fig. 1. The self-consistency requirements for the analysis necessitate an iterative procedure involving the two interconnected cycles, A and B, because *a priori* neither the true r_e structure nor the empirical harmonic frequencies are known. The generation of data for the input stream of the flow chart and the steps involved in cycles A and B warrant separate descriptions.

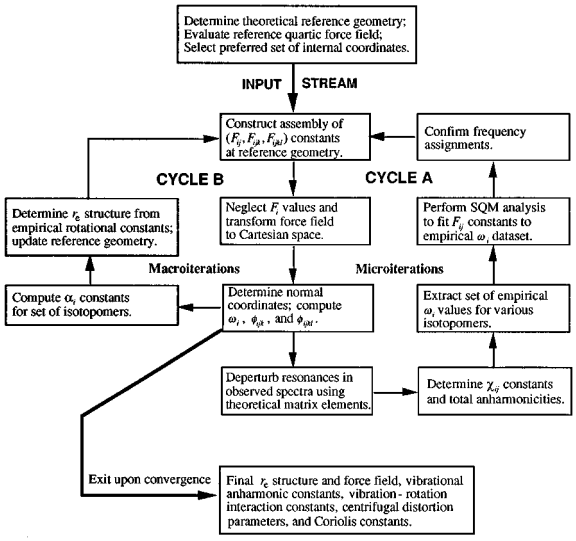

FIG. 1. Flowchart for anharmonic vibrational analysis of ketene isotopomers.

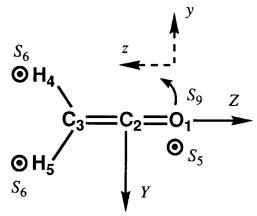

FIG. 2. Structural diagram for the internal coordinates of ketene. In addition to the atomic numbering and molecular axis system (X,Y,Z), sign conventions for the linear and out-of-plane bending variables of Table II are depicted. For $\theta_{x,y}(4,3,2,1)$ the local axis system (x,y,z) is affixed to the molecular framework, indicating that the positive directions for S_5 and S_9 involve the displacement of O_1 *out* of the plane of the figure ($+X$ direction) in the first instance and in the molecular plane *toward* H_4 in the second case. Displacements of H_4 and H_5 in the $+X$ direction lead to positive values for S_6, the CH_2 wagging coordinate.

A. Input stream

Initiation of the procedure requires the determination of a theoretical reference geometry which is expected with some confidence to be only slightly perturbed from the true r_e structure. For this purpose the QZ($2d1f,2p1d$) CCSD(T) structure was adopted, which is shown *post facto* in Table I to exhibit errors in r_e(C═O), r_e(C═C), r_e(C–H), and θ_e(H–C–H) of only $+0.0055$ Å, $+0.0068$ Å, $+0.0024$ Å, and $+0.11°$, respectively. The set of chemically intuitive internal symmetry coordinates selected for the analysis is specified in Table II with respect to the structural diagram in Fig. 2. It is noteworthy that the linear bending variables for the C═C═O moiety are defined with respect to the instantaneous plane of the methylene group and thus possess genuine rotational and translational invariance.

In the space of the preferred internal coordinates, a reference quartic force field was then obtained at the QZ($2d1f,2p1d$) CCSD(T) geometry by computing all the QZ($2d,2p$) MP2 cubic and quartic force constants and appending them to the corresponding set of QZ($2d,2p$) CCSD second derivatives. Because the relative contribution of electron correlation to force constants evaluated at a *fixed* reference structure generally diminishes as the order of the derivative increases,[102] the collection of QZ($2d,2p$) CCSD/MP2 predictions is expected to provide a good approximation to the true QZ($2d1f,2p1d$) CCSD(T) quartic force field, whose explicit computation was not feasible. Relevant data for diatomic carbon monoxide demonstrate the efficacy of this approximation. To wit, the QZ($2d,2p$) CCSD/MP2 values for f_{rr}, f_{rrr}, and f_{rrrr} at the QZ($2d1f,2p1d$) CCSD(T) optimum geometry ($r_e=1.1342$ Å) give ($\omega_e,\omega_e x_e$)=(2167.4, 12.48) cm^{-1}, whose propinquity to both the true QZ($2d1f,2p1d$) CCSD(T) results (2155.2, 11.70) cm^{-1} and their experimental[119] counterparts (2169.81, 13.29) cm^{-1} is gratifying. Moreover, differences in unscaled harmonic frequency predictions of such an extent are essentially of no consequence here because the *ab initio* quadratic force constants are eventually refined in the vibrational procedure to reproduce the set of observed fundamentals.

While the determination of the QZ($2d,2p$) CCSD//

TABLE II. Internal coordinate set for ketene.[a]

Coordinate	Irrep.	Scale factor[b]	Description
$S_1=2^{-1/2}[r(3,4)+r(3,5)]$	a_1	f_1	C–H symmetric stretch
$S_2=r(1,2)$	a_1	f_2	C=O stretch
$S_3=2^{-1/2}[\beta(2,3,4)+\beta(2,3,5)]$	a_1	f_3	CH_2 scissor
$S_4=r(2,3)$	a_1	f_4	C=C stretch
$S_5=2^{-1/2}[\theta_x(4,3,2,1)-\theta_x(5,3,2,1)]$	b_1	f_5	C=C=O linear bend
$S_6=\gamma(2,3,4,5)$	b_1	f_6	CH_2 wag
$S_7=2^{-1/2}[r(3,4)-r(3,5)]$	b_2	f_1	C–H antisymmetric stretch
$S_8=2^{-1/2}[\beta(2,3,4)-\beta(2,3,5)]$	b_2	f_7	CH_2 rock
$S_9=2^{-1/2}[\theta_y(4,3,2,1)-\theta_y(5,3,2,1)]$	b_2	f_8	C=C=O linear bend

[a]See the diagram in Fig. 2 for the assumed numbering of atoms and a depiction of sign conventions for the linear and out-of-plane bending coordinates. Definitions: $r(i,j)=i-j$ bond distance; $\beta(i,j,k)=i-j-k$ valence bond angle; $\gamma(i,j,k,l)$=angle of $i-j$ bond vector out of $j-k-l$ plane; $\theta_{x,y}(i,j,k,l)=x,y$ component of $k\rightarrow l$ unit vector in the local, right-handed coordinate system in which the $k\rightarrow j$ bond vector defines the z axis and atom i lies in the yz plane in the $+y$ direction. As such, θ_x and θ_y are dimensionless linear bending coordinates for which the bending planes are defined instantaneously by the molecular framework.

[b]Two independent scale factors (f_9 and f_{10}) for the off-diagonal quadratic constants F_{42} and F_{65} were also incorporated into the SQM analysis.

QZ($2d1f,2p1d$) CCSD(T) quadratic force field by standard finite-difference procedures requires no elaboration, details are warranted regarding the evaluation of the analogous QZ($2d,2p$) MP2 third and fourth derivatives. The following estimators[83] were utilized to determine the force constants F_{ijk} and F_{ijkl} in the internal space from analytic second derivatives F_{kl} computed at structures displaced from the reference geometry by $(\pm\Delta_i,\pm\Delta_j)$ in coordinates S_i and S_j:

$$F_{i,jk}=(2\Delta_i)^{-1}[F_{jk}(+\Delta_i)-F_{jk}(-\Delta_i)], \tag{1}$$

$$F_{ii,jk}=(\Delta_i)^{-2}[F_{jk}(+\Delta_i)+F_{jk}(-\Delta_i)-2F_{jk}(0)], \tag{2}$$

and

$$\begin{aligned}F_{ij,kl}=(2\Delta_i\Delta_j)^{-1}[&F_{kl}(+\Delta_i,+\Delta_j)+F_{kl}(-\Delta_i,-\Delta_j)\\&+2F_{kl}(0,0)-F_{kl}(+\Delta_i,0)-F_{kl}(-\Delta_i,0)\\&-F_{kl}(0,+\Delta_j)-F_{kl}(0,-\Delta_j)].\end{aligned} \tag{3}$$

The vibrational representation $4a_1\oplus 2b_1\oplus 3b_2$ for the internal space of ketene allows all constants of the type F_{ijk} and F_{iijk} to be evaluated via Eqs. (1) and (2) from F_{kl} sets at the reference point and 13 singly displaced structures. According to Eq. (3), the additional double displacements required to determine all F_{ijkl} constants are of the type $(+\Delta_i,+\Delta_j)$ and $(-\Delta_i,-\Delta_j)$ only. The estimator

$$\begin{aligned}F^{*}_{ij,kl}=(4\Delta_i\Delta_j)^{-1}[&F_{kl}(+\Delta_i,+\Delta_j)+F_{kl}(-\Delta_i,-\Delta_j)\\&-F_{kl}(+\Delta_i,-\Delta_j)-F_{kl}(-\Delta_i,+\Delta_j)]\end{aligned} \tag{4}$$

is an alternative to Eq. (3), but it requires essentially twice as many displacements and gives no improvement in accuracy. In particular, the analytical result

$$F_{ij,kl}-F^{*}_{ij,kl}=(1/4)F_{iijjkl}\Delta_i\Delta_j+O(\Delta^4) \tag{5}$$

reveals that the difference between the two quartic estimators is of the order of Δ^2, the same level of accuracy already provided by Eqs. (1)–(4).

Ostensibly the number of double displacements required by Eq. (3) is two for each (a_1,a_1), (a_1,b_1), and (a_1,b_2) pair and one for each (b_1,b_1), (b_1,b_2), and (b_2,b_2) combination, precisely a total of 62. However, if S_i and S_j belong to distinct irreducible representations, Γ_i and Γ_j, then F_{ijkl} is nonzero only if S_k belongs to Γ_i and S_l to Γ_j (or vice versa), in which case the $F_{ij,kl}$ estimator can be replaced by either of the two quantities among $F_{ik,jl}$, $F_{jl,ik}$, $F_{il,jk}$, and $F_{jk,il}$ involving a pair of either Γ_i or Γ_j coordinate displacements. Therefore, it is possible to limit the double displacements to the 16 pairs involving coordinates of the same irreducible representation. In this study the 40 displacements of (a_1,b_1) and (a_1,b_2) type were nevertheless included in the finite-difference procedure to ensure accuracy and internal consistency. The six remaining (b_1,b_2) displacements were discarded from the computation since it was not found possible to converge the associated F_{ij} sets with sufficient accuracy to overcome loss of significance in the resulting F_{ijkl} estimators, presumably because no molecular symmetry remains after such deformations. All quartic terms which vanish by symmetry were constrained to zero even though the form of Eq. (3) can lead to small residuals for certain estimators of these quantities. Each nonzero component of the final quartic force field was obtained by averaging over the collection of available estimators, which were tightly clustered due to the stringent convergence criteria employed in the analytic MP2 second derivative computations.[120] Representative of this internal consistency are the following sets of $F_{ij,kl}$ values for F_{ijkl} constants: F_{9865} {0.014 043 (98,65), 0.014 038 (65,98)} aJ rad^{-4}; F_{4422} {1.3702 (22,44), 1.3701 (44,22), 1.3678 (42,42)} aJ Å^{-4}; and F_{8743} {0.194 55 (87,43), 0.194 48 (84,73), 0.194 54 (83,74), 0.194 43 (43,87), 0.194 57 (73,84), 0.194 57 (74,83)} aJ Å^{-2} rad^{-2}.

B. Cycle A

In this interior cycle of the analysis, the reference geometry is held fixed while the quadratic force field is refined to self-consistency with the empirical fundamentals by means of several microiterations on the vibrational anharmonicities. The starting point of each iteration is the assembly of constants which comprise the quartic force field, these being generated at levels of theory which in general give residual gradients (F_i) at the assumed structure. These gradients are neglected in the representation of the preferred internal coordinates, a process which is equivalent to adding a linear shift term to the predicted potential energy surface to bring its equilibrium point into coincidence with the reference geometry.[102,121] The issues surrounding the determination of higher-order force constants at nonstationary reference geometries are explored in some detail in a recent article by Allen and Császár.[102]

The nonlinear transformation of the quartic force field from the internal to Cartesian space was implemented with the program INTDER.[102,122] Formulas for the higher-order B-matrix elements required in this transformation are generally known for common internal coordinate types,[123–126] and those for the linear bending variables employed here are available from the authors upon request. A normal coordinate analysis and subsequent transformation of the anharmonic Cartesian force field to the reduced normal coordinate representation yields the set of ω_i, ϕ_{ijk}, and ϕ_{ijkl} parameters needed to deperturb the vibrational resonances observed in the infrared spectra of ketene isotopomers. The identification and first-order treatment of these resonances is addressed in Sec. VI. In addition, the $\{\omega_i,\phi_{ijk},\phi_{ijkl}\}$ data facilitate the second-order computation[95,96,99] of the anharmonic constants χ_{ij}, in which contributions from the aforementioned resonance interactions are excluded. By subtracting the total anharmonicities ensuing from the χ_{ij} values from the previously deperturbed fundamentals, a set of empirical harmonic frequencies was ascertained. Those ω_i values which were both firmly established and internally consistent were accepted in the final data set, which in this study included all normal frequencies of H_2CCO, HDCCO, and D_2CCO, less ω_4 and ω_8 of the monodeuterated variant, as well as ω_2 and ω_8 of $H_2C^{13}CO$. Both of the included $H_2C^{13}CO$ frequencies exhibit sizeable carbon-13 shifts and solidify the information base for the methylene rocking and C═O stretching modes.

To upgrade the assumed quadratic force field, an SQM fit of scale factors to the set of ω_i values was performed. Significantly smaller residuals were obtained by ascribing separate parameters to all bending modes within the CH_2 and

C═C═O groups, but independent scale factors were not found necessary for the two C–H stretching vibrations. The resulting correlation of scale factors to internal coordinates is shown explicitly in Table II. It became apparent in the procedure that the SQM scheme of scaling off-diagonal force constants according to the geometric mean of the associated diagonal scale factors is overly restrictive for the C═C/C═O stretch interaction constant (F_{42}) and its counterpart involving the two b_1 bending modes (F_{65}). The principal and nonplussing manifestation of the SQM constraint in the F_{42} case was not a difficulty in reproducing the heavy-atom stretching fundamentals but the inability to collectively fit the C–H and C–D stretching frequencies to within 5 cm^{-1}, a consequence of the substantial degree of mixing with the C═O and C═C stretches which happens to occur in $\omega_1(D_2CCO)$ (see Table VII). Imbalanced scaling requirements arising from deficiencies in underlying *ab initio* force fields have indeed been documented previously,[89] particularly with regard to the stretch–stretch interaction constants in multiply bonded systems.[28,84,127–132] Accordingly, the final procedure adopted here for refining the quadratic force field on the set of 27 empirically based harmonic frequencies entailed the variation of 8 primary SQM scale factors plus the 2 independent off-diagonal constants F_{42} and F_{65}. From the updated quadratic force field in each iteration of cycle A, a modified set of anharmonicities and hence empirical harmonic frequencies results, providing the input data for the scaling procedure in the next cycle. Once a confirmed set of frequency assignments was established, self-consistency was always reached to better than 0.1 cm^{-1} within five iterations.

C. Cycle B

In this exterior cycle, the vibration–rotation interaction constants (α_i) resulting from the ω_i and ϕ_{ijk} constants converged in cycle A are used to compute the zero-point vibrational contributions to the high-precision rotational constants derived from microwave studies of ketene isotopomers. As detailed in Sec. X, these vibrational terms utilized in conjunction with analogous centrifugal distortion and electronic corrections yield sets of empirically based (A_e, B_e, C_e) values for H_2CCO, $H_2C^{13}CO$, $H_2{}^{13}CCO$, $H_2CC^{18}O$, HDCCO, and D_2CCO, from which an r_e structure of ketene is ascertained by established methods. The key facet of cycle B then involves shifting the reference point of the anharmonic force field expansion to this r_e structure. Once the assumed force field is shifted, iterations over cycle A are initiated once again. Within only a few macroiterations involving cycle B, the r_e structure derived from the output of cycle A becomes precisely equivalent to the input reference geometry for the anharmonic vibrational analysis.

Due to the proximity of the QZ($2d1f,2p1d$) CCSD(T) equilibrium geometry to the true r_e structure of ketene, the associated shifts in the predominant force constants are small and may be estimated without undue effort. For the quadratic and cubic force constants, it is assumed that

$$F_{ij}(\mathrm{CCSD}) = F^{\circ}_{ij}(\mathrm{CCSD}) + \sum_{k=1}^{4} F^{\circ}_{ijk}(\mathrm{MP2})\,\delta S_k \qquad (6)$$

and

$$F_{ijk}(\mathrm{MP2}) = F^{\circ}_{ijk}(\mathrm{MP2}) + \sum_{l=1}^{4} F^{\circ}_{ijkl}(\mathrm{MP2})\,\delta S_l, \qquad (7)$$

where the $\delta S_{k,l}$ quantities are the changes in the a_1 symmetry coordinates comprising the geometry shift, and the degree symbols denote the derivatives explicitly evaluated at the QZ($2d1f,2p1d$) CCSD(T) optimum structure. The implementation of first-order relationships is essentially exact for the range of $\delta S_{k,l}$ increments encountered here, and any inaccuracies arising in Eq. (6) from the use of MP2 rather than CCSD third derivatives are mitigated by the scaling procedure subsequently applied to the quadratic force field. Because the observed shift in the reference cubic constants proved to be only 2% on average, only the dominant stretching terms (F_{1111}, F_{2222}, F_{4444}, F_{7711}, and F_{7777}) in the quartic set were modified. For the C═O and C═C stretches, the simple correction $F_{kkkk} = F^{\circ}_{kkkk} + F^{\circ}_{kkkkk}\delta S_k$ was employed, an approximation recovering the actual shift to better than 1.5% in the cubic case, and for the symmetrized C–H stretching variables, the analogous estimate was $F_{1111} - F^{\circ}_{1111} = F_{7777} - F^{\circ}_{7777} = F_{7711} - F^{\circ}_{7711} = F^{\circ}_{11111}\delta S_1$, which derives from the general predominance of higher-order diagonal derivatives for individual bonds over associated stretch–stretch interaction terms. The required quintic force constants $\{F^{\circ}_{kkkkk};\ k=1,2,4\}$ were related to their third- and fourth-order counterparts by means of

$$F^{\circ}_{kkkkk} = \rho_k (F^{\circ}_{kkkk})^2 (F^{\circ}_{kkk})^{-1}, \qquad (8)$$

in which the values $(\rho_1,\rho_2,\rho_4) = (1.122, 1.10, 1.04)$ were utilized. For the C–H bonds, ρ_1 was explicitly evaluated by finite-difference procedures applied to QZ($2d,2p$) MP2 second derivatives, but for the C═O and C═C bonds it was deemed sufficient to simply surmise the ρ_k parameters from values clustered in the 1.0–1.2 range present in *ab initio* force fields of HNCO,[103] CO_2,[114] and C_2H_4.[99] By comparison, ρ_k equals (45/49) for all bonds within the Morse oscillator approximation, which appears to be a modest underestimation for the bond types of current concern.

IV. FORCE FIELD AND NORMAL VIBRATION FREQUENCIES

The converged QZ($2d,2p$) SQM(CCSD)//EXPT quadratic force constants and harmonic frequencies for the normal vibrations of ketene are given in Table III and compared therein to other sets of theoretical and empirical results. The associated QZ($2d,2p$) MP2//EXPT cubic and quartic force constants in both the internal and reduced normal coordinate representations are collected in Tables IV and V. Tabulations of ϕ_{ijk} and ϕ_{ijkl} constants for D_2CCO and HDCCO are provided as supplementary material.[133] To facilitate interpretation of the force constants, the variables in Table II are numbered such that the principal component of each reduced normal coordinate q_i for the parent and deuterated isotopomers is simply the internal coordinate S_i. The only instance in which this construction is not possible is the strongly mixed b_1 pair (ω_5,ω_6) of H_2CCO, for which the preferred assignments are the C═C═O linear bend and CH_2

TABLE III. Quadratic force constants (F_{ij}) and harmonic vibrational frequencies (ω_i) of H_2CCO.[a,b]

		DZP CISD// DZP CISD[c]	QZ($2d,2p$) MP2// QZ($2d1f,2p1d$) CCSD(T)	QZ($2d,2p$) CCSD// QZ($2d1f,2p1d$) CCSD(T)	Empirical GHFF[d]	QZ($2d,2p$) SQM(CCSD)// EXPT[e]
11	(a_1)	6.2185	5.8518	5.8116	5.880	5.8414
21		−0.0973	−0.1079	−0.0891	[−0.080]	−0.0881
22		17.2981	15.6562	15.5527	15.44	15.7467
31		−0.0699	−0.0536	−0.0541	[−0.064]	−0.0513
32		−0.0106	−0.0114	−0.0161	[0.000]	−0.0154
33		1.3064	1.2178	1.2530	1.206	1.1939
41		0.0889	0.1076	0.1255	0.131	0.1211
42		0.7914	0.5715	0.7955	0.551	0.5995
43		0.4835	0.4746	0.4635	0.393	0.4434
44		10.1129	9.3820	9.4140	9.244	9.4040
55	(b_1)	0.3461	0.3054	0.3175	0.3342	0.31351
65		0.0756	0.0709	0.0724	0.0677	0.07043
66		0.0915	0.0712	0.0874	0.0879	0.08366
77	(b_2)	6.2036	5.8313	5.7730	5.784	5.8029
87		0.1832	0.1971	0.1913	0.1605	0.1870
88		0.4176	0.3881	0.4096	0.3751	0.3852
97		0.0069	0.0034	0.0072	[0.000]	0.0078
98		0.0976	0.0958	0.0922	0.0944	0.0887
99		0.3325	0.2896	0.3017	0.3240	0.2999
ω_1	(a_1)	3305	3205	3194	3211	3202.2
ω_2		2284	2194	2170	2181	2197.2
ω_3		1477	1419	1442	1422	1415.2
ω_4		1197	1147	1156	1133	1146.0
ω_5	(b_1)	606	564	590	592	581.9
ω_6		529	457	507	536	502.6
ω_7	(b_2)	3422	3316	3300	3306	3308.2
ω_8		1036	999	1018	996	996.0
ω_9		453	420	436	442	433.6

[a]The units of the force constants are consistent with energy in aJ, bond lengths in Å, and bond angles in radians; harmonic frequencies in cm^{-1}. The internal coordinate set for the F_{ij} values is defined in Table II.

[b]To fully specify the force fields for mathematical transformations, the first derivatives (F_i) at the QZ($2d1f,2p1d$) CCSD(T) reference structure must be specified. The F_i values in aJ $Å^{-1}$ are: MP2 1(0.025 010), 2(−0.006 157), 3(0.003 438), 4(0.017 154); and CCSD 1(0.020 071), 2(0.099 110), 3(0.002 573), 4(0.038 001).

[c]Reference 134.

[d]Reference 28, constrained values in brackets.

[e]The experimental reference geometry is structure r_e(I) of Table I.

wag, respectively, whereas the reverse is true for the deuterated analogs (see Table VI). As a consequence of the present numbering scheme and full symmetrization of all simple internal coordinates, various permutations, sign changes, and rescalings of previous quadratic force constants are required for the comparison in Table III. In particular, $\{S_1,S_2,S_3,S_4,S_5,S_6,S_9\}$ in the DZP CISD//DZP CISD analysis of Allen and Schaefer[134] correlate to $\{S_2,S_4,S_1,S_3,S_6,S_5/\sqrt{2},S_9/\sqrt{2}\}$ here, while $\{S_2,S_3,S_4,S_5,S_8,S_9\}$ in the empirical GHFF of Duncan *et al.*[28] become $\{S_4,S_2,-\sqrt{2}S_3,S_5/\sqrt{2},-S_8/\sqrt{2},S_9/\sqrt{2}\}$.

In Table III the general agreement of the empirical GHFF and SQM(CCSD)//EXPT harmonic frequencies with the QZ($2d,2p$) MP2 and CCSD predictions computed at the QZ($2d1f,2p1d$) CCSD(T) optimum structure validates the reference force field employed in the vibrational procedure of this study. Nevertheless, disparate levels of agreement are observed among the ω_i values for those modes [group A: (1,2,3,4,7,8)] in which the linear C═C═O framework is essentially preserved vs the complementary modes involving substantial deformations of this moiety [group B:(5,6,9)]. As compared to the final SQM(CCSD)//EXPT frequencies, the error range of the QZ($2d,2p$) MP2//QZ($2d1f,2p1d$) CCSD(T) predictions for group A is $[-3.8, +7.9]$ cm^{-1} with an average absolute deviation of only 3.7 cm^{-1}, whereas the analogous errors for group B are $(-18, -46, -14)$ cm^{-1}, a factor of 7 larger on average. Conversely, the QZ($2d,2p$) CCSD//QZ($2d1f,2p1d$) CCSD(T) error range for group A is $[-27.8, +27.3]$ cm^{-1} with an average absolute deviation of 17.1 cm^{-1}, while much better agreement is observed for group B, the errors being $(+8, +4, +2)$ cm^{-1}. The exceptional accuracy of the QZ($2d,2p$) MP2//QZ($2d1f,2p1d$) CCSD(T) bond stretching frequencies is clearly attributable to the use of reference bond lengths which are slightly longer than experiment,[102] balancing with fortuitously good precision the overestimations which would otherwise result from deficiencies of the basis set and electron correlation treatment. By comparison, the earlier ω_i values given by the DZP CISD level of theory[134] are tightly clustered between 3.2% and 5.3% above their SQM(CCSD)//EXPT counterparts, despite the proximity of the DZP CISD equilibrium geometry

TABLE IV. Cubic force constants of H_2CCO.[a,b]

ijk	F°_{ijk}[a]	F_{ijk}	ϕ_{ijk}	ijk	F°_{ijk}	F_{ijk}	ϕ_{ijk}
111	−23.0120	−23.2917	−1321.03	661	−0.1907	−0.1902	523.71
211	−0.0375	−0.0367*	41.17	662	0.1380	0.1390	125.03
221	0.0510	0.0490*	21.81	663	0.7526	0.7583	1.61
222	−107.8994	−111.6545	−334.06	664	−0.1121	−0.1107	56.36
311	0.1546	0.1529	76.22	771	−23.2332	−23.5221	−1412.36
321	−0.0394	−0.0396*	46.80	772	−0.0366	−0.0371*	25.04
322	−0.0034	−0.0036*	190.25	773	−0.4112	−0.4126	−46.19
331	−0.7366	−0.7376	264.66	774	0.2078	0.2142	−56.73
332	−0.1244	−0.1268	12.52	871	0.0428	0.0426*	62.62
333	0.3965	0.3907	62.20	872	0.0002	0.0015*	50.62
411	0.1812	0.1927	−25.58	873	−0.1933	−0.1943	330.03
421	0.1620	0.1664	−17.74	874	−0.3954	−0.3923	82.49
422	−2.0165	−2.0902	−353.39	881	−0.2634	−0.2639	274.74
431	−0.3775	−0.3783	52.69	882	−0.1383	−0.1410	−47.84
432	−0.0088	−0.0087*	−47.87	883	−0.3713	−0.3716	−108.27
433	0.0016	0.0074*	−42.64	884	0.2227	0.2280	6.91
441	−0.1008	−0.0848*	42.14	971	0.0029	0.0029*	−46.06
442	−1.9590	−1.9868	50.91	972	−0.0273	−0.0282*	−29.26
443	0.0786	0.0772*	112.43	973	−0.0298	−0.0306*	−426.57
444	−55.1206	−56.9985	−172.29	974	−0.0967	−0.0987*	−142.52
551	−0.0181	−0.0177	690.60	981	−0.0478	−0.0490	−416.88
552	−0.6676	−0.6793	66.76	982	−0.0915	−0.0913	66.18
553	−0.0367	−0.0363	157.74	983	−0.0848	−0.0853	18.21
554	−0.6378	−0.6500	120.91	984	0.0062	0.0079*	29.08
651	0.0340	0.0340	−618.29	991	−0.0095	−0.0089*	537.04
652	−0.0467	−0.0464	22.42	992	−0.5120	−0.5183	105.70
653	0.1222	0.1213	−144.95	993	0.0052	0.0044*	−64.16
654	0.1457	0.1456	2.52	994	−0.3684	−0.3767	120.25

[a]The reference F°_{ijk} constants are explicit QZ($2d,2p$) MP2//QZ($2d1f,2p1d$) CCSD(T) results, while the final F_{ijk} values include a correction which modifies the reference geometry to structure r_e(I) of Table I. See footnote a of Table III for units of the F_{ijk} sets; the internal coordinates are defined in Table II. The ϕ_{ijk} constants in the reduced normal coordinate representation are given in cm^{-1}; the phases of the associated normal coordinates are selected to be coincident with the positive direction of the predominant internal coordinate of each mode.

[b]Asterisks are affixed to those F_{ijk} elements which contribute negligibly to the vibrational anharmonic constants χ_{ij}.

(Table I) to the present QZ($2d1f,2p1d$) CCSD(T) reference structure.

A subtle dependence of harmonic frequencies on the totally symmetric nuclear coordinates utilized in the normal mode analysis is inherent in vibrational procedures at reference points which are not stationary at the chosen level of theory,[83,102,121] as in the QZ($2d,2p$) MP2 and CCSD cases. Conceivable alternatives to the *internal* set assumed here are not chemically realistic, however. Implementation of a Cartesian projection scheme[102] as an optional approach yields the following results for ω_1–ω_9 (cm^{-1}): QZ($2d,2p$) MP2 (3205, 2194, 1429, 1148, 570, 473, 3316, 1006, 423) and QZ($2d,2p$) CCSD (3194, 2170, 1450, 1157, 620, 526, 3300, 1026, 472). The only significant variances with the corresponding entries in Table III occur for the group B modes, the differences being most pronounced in the CCSD case. In essence, the expected deterioration in frequency predictions resulting from rectilinear Cartesian rather than curvilinear internal projection is magnified for deformations of the linear C═C═O chain.

The empirical GHFF harmonic frequencies scatter above and below the final SQM(CCSD)//EXPT values converged in the present analysis, yet no difference exceeds 1.2% within group A. For the group B frequencies ($\omega_5,\omega_6,\omega_9$), the GHFF differences are significantly larger, viz., 1.7%, 6.6%, and 1.9%, respectively. The assumption of negative anharmonicities of 1% for C═C═O bending and 2% for methylene wagging modes in the GHFF refinement[28] is the apparent source of this disparity, because the procedure implemented here yields positive anharmonicities of 1.2%, 5.2%, and 1.2%, in order, for ω_5, ω_6, and ω_9, in large part due to the Coriolis effects described in Sec. V.

The individual elements of the quadratic force fields in Table III exhibit remarkable agreement overall. The tabulated diagonal constants closely mimic the aforementioned frequency trends. For example, the empirical GHFF values of F_{22} and F_{44} for the C═O and C═C stretches are ~2% smaller than the final quantities derived here, and the associated constants for the C═C═O bending modes are 5%–8% larger than their SQM(CCSD)//EXPT counterparts. The converged SQM scale factors for the shifted QZ($2d,2p$) CCSD//EXPT force field, with corresponding standard errors of the fit in parentheses, are f_1(C–H str.)=0.9915(8), f_2(C═O str.)=0.9744(24), f_3(CH_2 scissor)=0.9499(23), f_4(C═C str.)=0.9598(43), f_5(C═C═O bend)=0.9632(28), f_6(CH_2 wag)=0.9391(29), f_7(CH_2 rock)=0.9410(30), and f_8(C═C═O bend)=0.9768(45), all of which lie slightly below 1.0, as expected for this level of theory. The apparent occurrences of scale factors greater than unity implied by certain QZ($2d,2p$) CCSD//QZ($2d1f,2p1d$) CCSD(T) →QZ($2d,2p$) SQM(CCSD)//EXPT differences in Table III are merely manifestations of the reference geometry shift.

TABLE V. Quartic force constants of H_2CCO.[a,b]

$ijkl$	F_{ijkl}[a]	ϕ_{ijkl}	$ijkl$	F_{ijkl}	ϕ_{ijkl}	$ijkl$	F_{ijkl}	ϕ_{ijkl}	$ijkl$	F_{ijkl}	ϕ_{ijkl}	$ijkl$	F_{ijkl}	ϕ_{ijkl}
1111	[83.501]	492.25	4443	0.3722	−16.27	6644	−0.0855	−19.94	8821	−0.0046*	5.51	9832	0.0952*	−16.60
2111	−0.0426*	−13.93	4444	[285.99]	28.40	6655	0.2055	488.28	8822	0.3232	−27.68	9833	0.0169*	−142.24
2211	−0.1039*	−0.59	5511	−0.0477	−407.54	6665	0.1651	−396.35	8831	0.2767	46.83	9841	0.1696*	−2.27
2221	0.2830*	6.86	5521	−0.0140*	5.92	6666	1.7972	533.09	8832	0.2800	12.30	9842	0.0886*	−9.05
2222	[693.05]	164.58	5522	0.9279	−42.24	7711	[85.564]	535.68	8833	0.1659	96.91	9843	−0.0249	−31.04
3111	−0.0992*	−47.38	5531	−0.0221*	−32.24	7721	−0.0360*	−12.66	8841	0.1669	15.24	9844	−0.4387	−22.28
3211	0.0182*	−13.90	5532	−0.0173*	3.85	7722	−0.1490*	−2.46	8842	0.1909	15.08	9855	−0.0245	−82.91
3221	−0.1044*	2.87	5533	0.0041*	31.34	7731	0.1548*	−3.86	8843	−0.2852	35.30	9865	0.0140	89.76
3222	−0.3797	−12.43	5541	−0.0252*	−27.68	7732	−0.0936*	−18.25	8844	−1.0872	−4.52	9866	0.0658	−64.93
3311	0.0245*	−214.07	5542	0.9886	−10.69	7733	−1.2527	−266.92	8855	−0.0343	47.40	9877	−0.0749	264.37
3321	−0.1133*	6.94	5543	−0.0366	12.18	7741	−0.9790	15.41	8865	−0.0219	−49.91	9887	0.0939*	−38.98
3322	0.2422	13.43	5544	1.0102	−7.15	7742	0.2005*	−5.46	8866	0.0730	26.40	9888	−0.0577	−104.77
3331	−0.5858	1.58	5555	1.9313	598.94	7743	−0.0526*	−90.63	8877	−0.0775	−223.56	9911	−0.0429	−301.27
3332	0.2387	6.27	6511	−0.0155*	365.31	7744	−0.6117	−31.28	8887	0.2973	50.36	9921	−0.0887*	8.01
3333	0.0758	50.60	6521	−0.0393*	−5.94	7755	−0.0392*	−456.50	8888	−0.1612	72.47	9922	0.3102	−90.71
4111	−1.3174	−1.27	6522	−0.0386	−49.90	7765	−0.0054*	415.03	9711	−0.0453*	38.88	9931	−0.0469*	32.64
4211	−0.0097*	−5.53	6531	−0.0036*	15.46	7766	−0.3480	−377.03	9721	−0.0053*	17.92	9932	0.0231*	22.68
4221	0.0912*	−4.83	6532	−0.1206	2.68	7777	[86.494]	565.53	9722	0.0425*	1.78	9933	0.0728	171.66
4222	11.7763	26.78	6533	−0.0133	−47.61	8711	−0.3684*	−40.95	9731	−0.0340*	271.35	9941	−0.0024*	−1.51
4311	0.2820*	−72.63	6541	0.0334	18.76	8721	0.0058*	−14.25	9732	0.0487*	−5.72	9942	0.7185	−13.55
4321	0.0896*	−1.98	6542	−0.0215*	−7.70	8722	−0.0849*	3.17	9733	0.0478*	3.41	9943	0.1425	68.32
4322	0.4430	−29.11	6543	0.2398	−8.03	8731	−0.0662*	−225.82	9741	0.0169*	92.75	9944	0.6680	−4.20
4331	0.1182*	−8.29	6544	0.0673	−16.31	8732	0.0248*	7.51	9742	0.1108*	−4.52	9955	0.4119	125.42
4332	0.2645	−3.63	6555	0.0079*	−492.33	8733	0.1825*	10.24	9743	0.0917*	9.08	9965	0.0366	−89.95
4333	0.9858	10.55	6611	0.1279	−329.70	8741	0.2083*	−77.22	9744	0.2055*	9.83	9966	0.1637	101.43
4411	−0.9542	−23.52	6621	0.0086*	−3.98	8742	−0.1182*	−0.36	9755	0.0116*	10.12	9977	−0.0121*	−314.01
4421	−0.7129	6.15	6622	−0.1695	−80.01	8743	0.1945*	−3.01	9765	−0.0071*	−2.14	9987	−0.0520*	21.66
4422	1.3686	51.66	6631	−0.7171	−7.32	8744	−0.4293*	−1.93	9766	−0.0345*	−5.77	9988	0.1421	172.94
4431	−0.0781*	−1.15	6632	0.2261	1.33	8755	−0.0282*	−4.74	9777	−0.0666*	−18.88	9997	0.0589*	−10.38
4432	−0.3816	12.42	6633	3.1842	39.51	8765	−0.0086*	−10.87	9811	−0.0628	246.79	9998	−0.0296	−206.54
4433	−0.9443	14.70	6641	−0.2984	−5.30	8766	−0.0408*	21.04	9821	0.0639*	−14.16	9999	0.9703	369.65
4441	−1.3145	−7.49	6642	0.0310	8.70	8777	−0.4930*	6.14	9822	−0.1696	−44.25			
4442	3.2997	−14.14	6643	−0.0256	32.16	8811	−0.0681	−207.08	9831	0.0473*	−43.70			

[a]See footnote a of Table III for units of the F_{ijkl} values; the internal coordinate set is defined in Table II. The F_{ijkl} constants are explicit QZ($2d,2p$) MP2//QZ($2d1f,2p1d$) CCSD(T) results except those appearing in brackets, which include a correction to shift the reference geometry to structure r_e(I) of Table I. The corresponding unshifted F_{ijkl} values are 1111(82.342), 2222(668.025), 4444(276.27), 7711(84.405), and 7777(85.335). The ϕ_{ijkl} constants are listed in cm^{-1}, and the phases of the associated reduced normal coordinates are the same as those in Table IV.

[b]Asterisks are affixed to those F_{ijkl} elements which contribute negligibly to the vibrational anharmonic constants χ_{ij}.

The consistency among the tabulated off-diagonal force constants provides general confirmation of the previous empirical values, and in particular the constraints imposed on F_{21}, F_{31}, F_{32}, and F_{97} in the GHFF fit.

The only term exhibiting variations of some severity in Table III is the C═O/C═C stretch interaction constant (F_{42}). In both the DZP CISD and QZ($2d,2p$) CCSD cases, this constant is overestimated by about 30%, and the corresponding off-diagonal scale factor (f_9=0.7318) converged in the present vibrational procedure is thus small. However, the QZ($2d,2p$) MP2 prediction for F_{42} happens to be in excellent agreement with both the empirical GHFF and SQM(CCSD)//EXPT quantities, even though MP2 theory actually overshoots the true correlation component of F_{42} to some degree. In addition, previous studies of ketene[28,134] reveal that RHF values for F_{42} obtained with polarized basis sets are too large by at least a factor of 2. Data for the quadratic C═O/C═O stretch interaction constant ($f_{rr'}$) of carbon dioxide provide a clear precedent for these occurrences.[100,114,115] Specifically, the TZ2P RHF and TZ2P CISD values for $f_{rr'}(CO_2)$ reported by Allen *et al.*[100] at the corresponding theoretical equilibrium structures are 2.342 and 1.754 aJ $Å^{-2}$, in order, as compared to the 0.944 aJ $Å^{-2}$ result given by the current QZ($2d,2p$) MP2//EXPT procedure. Experimental refinements place $f_{rr'}$ near 1.253 aJ $Å^{-2}$,[135] a value supported by a recent, high-quality *ab initio* prediction[115] of 1.230 aJ $Å^{-2}$ determined with the cc-pVQZ CCSD(T) method. In contrast to F_{42}, the various entries in Table III for the interaction constant (F_{65}) coupling the two b_1 bending modes are quite uniform, although both the SQM(CCSD)//EXPT result and the unscaled *ab initio* data suggest that the GHFF value for F_{65} is slightly low. The final SQM(CCSD)//EXPT constant corresponds to an off-diagonal scale factor (f_{10}=0.9826) near unity. It is only the relative sensitivity of the b_1 harmonic frequencies to F_{65} which merits the use of an independent scale factor in the vibrational procedure.

The accurate set of quadratic force constants and harmonic vibrational frequencies established for ketene facilitates detailed chemical characterizations by means of spectroscopic comparisons unfettered from anharmonic vibrational effects, including resonance interactions. The unusually small diagonal force constant for methylene wagging in ketene (F_{66}=0.0837 aJ rad^{-2}) is only about one-third of

TABLE VI. Vibrational anharmonic constants χ_{ij} (cm^{-1}) for H_2CCO and D_2CCO.[a]

	H_2CCO					D_2CCO				
ij	χ_{ij}		Σ_1	Σ_2	Σ_3	χ_{ij}		Σ_1	Σ_2	Σ_3
11	−26.66		(30.77,	−57.43,	0)	−11.88		(11.56,	−23.44,	0)
21	−2.04		(−0.15,	−1.90,	0)	−11.76		(12.06,	−23.82,	0)
22	−11.15		(10.29,	−21.44,	0)	−8.56		(8.11,	−16.67,	0)
31	−5.70		(−53.52,	47.81,	0)	−22.24		(−4.63,	−17.61,	0)
32	−4.76		(3.36,	−8.12,	0)	−8.95*	[29.11]	(8.99,	−17.94,	0)
33	−6.29		(3.16,	−9.45,	0)	1.16		(2.29,	−1.14,	0)
41	−3.85		(−5.88,	2.03,	0)	−7.53		(−17.34,	9.81,	0)
42	−13.97		(12.92,	−26.88,	0)	−2.90*	[35.16]	(−0.71,	−2.19,	0)
43	−2.88		(3.67,	−6.56,	0)	−3.01*	[−41.07]	(3.35,	−6.36,	0)
44	−1.15		(1.78,	−2.92,	0)	−0.82		(0.79,	−1.61,	0)
51	−5.87		(−101.88,	95.73,	0.29)	−2.46		(−4.99,	2.40,	0.13)
52	−4.25		(−10.56,	5.79,	0.52)	−9.27		(−24.16,	13.75,	1.14)
53	11.12		(7.83,	2.87,	0.42)	3.98		(−7.20,	11.18,	0.00)
54	−3.78**	[−106.8]	(−1.79,	−2.03,	0.04)	−1.42**	[−13.9]	(−2.06,	0.60,	0.03)
55	0.28*	[26.02]	(37.43,	−37.15,	0)	2.92*	[3.19]	(7.79,	−4.87,	0)
61	−8.81		(−82.43,	73.33,	0.28)	−8.41		(−86.18,	77.16,	0.62)
62	−9.83		(−20.00,	9.22,	0.95)	−1.59		(−13.81,	12.22,	0.01)
63	6.78		(9.88,	−3.39,	0.30)	−4.46		(1.77,	−6.57,	0.34)
64	−5.53**	[−2.70]	(−4.98,	−0.54,	0.00)	−1.94**	[7.47]	(8.06,	−10.23,	0.25)
65	14.92*	[14.91]	(122.06,	−107.15,	0)	5.30*	[16.66]	(9.08,	−3.78,	0)
66	14.83*	[14.12]	(33.32,	−18.48,	0)	13.02*	[7.82]	(64.00,	−50.98,	0)
71	−112.25		(133.92,	−246.17,	0.00)	−51.81		(62.66,	−114.49,	0.02)
72	−0.14*	[2.65]	(−0.61,	0.47,	0.00)	−7.92		(8.56,	−16.49,	0.00)
73	−18.42		(−66.73,	47.48,	0.83)	−0.25		(−14.17,	13.65,	0.28)
74	−3.41		(−7.82,	4.31,	0.10)	−11.23		(−26.63,	14.89,	0.50)
75	−10.42		(−114.12,	78.74,	24.96)	−0.88		(−0.64,	−0.36,	0.13)
76	−16.05		(−94.26	58.10,	20.11)	−16.53		(−113.98,	75.03,	22.43)
77	−31.17		(35.35,	−66.52,	0)	−18.40		(19.54,	−37.94,	0)
81	−9.94		(−51.77,	41.09,	0.73)	−5.43		(−15.10,	9.02,	0.65)
82	−3.28*	[−6.07]	(−6.92,	3.37,	0.28)	−5.14		(−10.76,	5.46,	0.16)
83	−9.06*	[−11.94]	(24.23,	−33.29,	0.00)	−8.08*	[−5.64]	(−2.15,	−5.93,	0.00)
84	−1.25		(−1.13,	−0.16,	0.04)	−1.04		(3.46,	−4.54,	0.04)
85	0.45		(11.85,	−11.61,	0.21)	3.43		(−0.93,	−1.02,	5.37)
86	8.02		(6.60,	−10.61,	12.02)	−0.21		(2.03,	−3.86,	1.62)
87	−12.03*	[−9.24]	(−55.89,	43.85,	0)	−5.22		(−17.16,	11.94,	0)
88	−1.83		(4.53,	−6.36,	0)	0.18		(0.95,	−0.77,	0)
91	−1.22		(−75.32,	73.27,	0.83)	−0.86		(−41.14,	39.94,	0.34)
92	−5.96		(−22.68,	15.04,	1.17)	−3.44		(−24.11,	19.28,	1.40)
93	−0.86*	[−3.73]	(42.91,	−43.78,	0.00)	0.46*	[2.91]	(6.55,	−6.09,	0.00)
94	4.06		(−1.05,	5.11,	0.00)	0.69		(18.11,	−17.42,	0.00)
95	10.89		(31.36,	−31.14,	10.68)	6.04		(5.36,	−4.24,	4.92)
96	3.76		(25.36,	−24.92,	3.32)	0.25		(31.66,	−32.17,	0.76)
97	−1.89		(−78.50,	76.61,	0)	−2.84		(−51.01,	48.17,	0)
98	−1.45*	[1.42]	(43.24,	−44.68,	0)	−1.58*	[−4.02]	(14.95,	−16.52,	0)
99	0.68		(23.10,	−22.42,	0)	0.66		(17.37,	−16.71,	0)

[a]Derived from the QZ(2*d*,2*p*) SQM(CCSD)+MP2//EXPT quartic force field. In parentheses the decomposition of the χ_{ij} values is shown into the successive terms appearing in Eqs. (9) and (10). Asterisks denote χ_{ij} constants deperturbed of the resonances identified in the text, whose effects are manifested in the adjacent values in brackets, which include all interaction terms in the second-order perturbation equations.

the magnitude found in ethylene, as first noted by Moore and Pimentel in 1963,[17] and just over half that occurring in allene.[136] Accordingly, $\omega_5(H_2CCO)=582$ cm^{-1} is much smaller than both its ω_7(ethylene) counterpart and the degenerate ω_{10}(allene), which lie near 970 and 860 cm^{-1}, respectively.[136,137] For the in-plane C═C═O bending mode of ketene, the diagonal force constant ($F_{99}=0.300$ aJ rad^{-2}) is almost 25% smaller than the corresponding value in carbon dioxide, contributing to a harmonic frequency ($\omega_9=434$ cm^{-1}) nearly 240 cm^{-1} lower than $\omega_2(CO_2)$.[135,138] In fact, early spectroscopic studies of ketene erroneously placed the ν_9 fundamental at substantially higher frequencies,[3–5,10–12] and the correct assignment was not ascertained until the advent of matrix-isolation spectroscopy.[17] The relatively flat C═C═O in-plane bending potential in ketene appears to presage the structurally anomalous behavior of higher cumulenones, which is manifested in the case of propadienone by equivalent, kinked equilibrium conformations with an attendant barrier of 1.0 kcal mol^{-1} to C═C═C═O linearity.[139]

Selected comparisons for the higher-frequency modes of ketene vis-à-vis ethylene,[137] allene,[136] and carbon dioxide[135,138] are also instructive. The relatively large C–H stretching frequencies in ketene, ω_1 and ω_7, are 40–50 and 70–90 cm^{-1}, respectively, higher than analogous values for

ethylene, the counterparts in allene being exceeded by similar amounts. The F_{22}(ketene) constant is only 1.7% smaller than $f_{rr}(CO_2)$, yet the associated C═O stretching frequency is almost 200 cm^{-1} below $\omega_3(CO_2)$. The CH_2 scissor in ketene (ω_3) appears to be within 10 cm^{-1} of ω_7(allene), while the CH_2 rock (ω_8) is less than the degenerate ω_9(allene) by just over 20 cm^{-1}. Finally, the deperturbation and harmonization of the C═C stretching fundamental of ketene yields an ω_4 value (1146 cm^{-1}) probably 50–60 cm^{-1} higher than ω_3(allene).

Assessment of the cubic and quartic force constants in Tables IV and V is greatly facilitated by previous systematic *ab initio* studies of vibrational anharmonicity.[99–102] The particular reliability of dominant diagonal constants and the validity of most off-diagonal components is to be expected if the computation involves an accurate reference structure and even a moderate level of theory—a standard which is certainly attained by the present QZ(2*d*,2*p*) MP2//EXPT predictions. Among the troublesome quantities to pinpoint theoretically are higher-order stretch–stretch interaction terms,[101,102] which in many cases are also poorly determined by the observable experimental data. As anticipated, the C═O/C═C interaction constants are the largest of this type for ketene, a calibration of which is made ineluctable by the recalcitrance of the quadratic constant F_{42} toward theoretical prediction. For this purpose the carbon dioxide benchmark is especially apt, since current QZ(2*d*,2*p*) MP2//EXPT predictions may be compared to recent QZ(2*d*,2*p*) CCSD(T)//EXPT[114] and cc-pVTZ CCSD(T)[115] theoretical results as well as preferred empirical values of relevant stretching force constants.[135] Collections of pertinent CO_2 data (aJ $Å^{-3}$ or aJ $Å^{-4}$ units) from these four sources, in the order mentioned, are as follows: f_{rrr}=(−111.9, −116.4, −112.6, −116.1), $f_{rrr'}$=(−3.1, −2.5, −2.7, −2.9), f_{rrrr}=(712.7, 693.2, 639.3, 656.1), $f_{rrrr'}$=(10.4, 4.0, 9.5, 8.3), and $f_{rrr'r'}$=(−3.0, 2.4, 1.2, 0.8). For f_{rrr}, $f_{rrr'}$, and f_{rrrr}, the QZ(2*d*,2*p*) MP2//EXPT method gives excellent reproduction of the other high-quality results, while for the less important $f_{rrrr'}$ and $f_{rrr'r'}$ terms the corresponding predictions are certainly satisfactory considering the general uncertainty attending these elements. The QZ(2*d*,2*p*) MP2//EXPT force constants for ketene analogous to those listed for carbon dioxide are F_{222}=−111.7, (F_{422},F_{442})=(−2.1, −2.0), F_{2222}=693.0, (F_{4222},F_{4442})=(11.8, 3.3), and F_{4422}=1.4, in the same order and units. The similarity of these values to their CO_2 analogs strongly suggests that the level of accuracy observed for carbon dioxide is maintained for ketene.

V. VIBRATIONAL ANHARMONICITIES AND FUNDAMENTAL FREQUENCIES

In Table VI vibrational anharmonic constants (χ_{ij}) derived from the final QZ(2*d*,2*p*) SQM(CCSD)+MP2//EXPT quartic force field are listed for H_2CCO and D_2CCO. As documented in a supplementary tabulation,[133] very similar albeit distinguishable χ_{ij} results are obtained from the unmodified QZ(2*d*,2*p*) CCSD+MP2//QZ(2*d*1*f*,2*p*1*d*) CCSD(T) reference force constants. To elucidate the factors governing the χ_{ij} values, decompositions are provided in Table VI into the total quartic (Σ_1), cubic (Σ_2), and Coriolis (Σ_3) contributions comprising the successive terms in braces in the following formulas:[95,96]

$$\chi_{ii}=\Sigma_1+\Sigma_2=\left\{\frac{1}{16}\,\phi_{iiii}\right\}+\left\{-\frac{5}{48}\,\frac{\phi_{iii}^2}{\omega_i}-\frac{1}{16}\sum_i{}^{*}\,\frac{\phi_{iij}^2(8\omega_i^2-3\omega_j^2)}{\omega_i(4\omega_i^2-\omega_j^2)}\right\} \tag{9}$$

and

$$\begin{aligned}\chi_{ij}&=\Sigma_1+\Sigma_2+\Sigma_3\\&=\left\{\frac{1}{4}\,\phi_{iijj}\right\}+\left\{-\frac{1}{4}\sum_k\,\frac{\phi_{iik}\phi_{kjj}}{\omega_k}-\frac{1}{2}\sum_k{}^{*}\,\frac{\phi_{ijk}^2\omega_k(\omega_k^2-\omega_i^2-\omega_j^2)}{[(\omega_i+\omega_j)^2-\omega_k^2][(\omega_i-\omega_j)^2-\omega_k^2]}\right\}\\&\quad+\left\{[A_e(\zeta_{ij}^a)^2+B_e(\zeta_{ij}^b)^2+C_e(\zeta_{ij}^c)^2]\left(\frac{\omega_i}{\omega_j}+\frac{\omega_j}{\omega_i}\right)\right\}.\end{aligned} \tag{10}$$

Through the Σ_2 components, resonances of the type (ω_i,$2\omega_j$) and (ω_i,$\omega_j+\omega_k$) adversely affect the $\{\chi_{ij},\chi_{jj}\}$ and $\{\chi_{ij},\chi_{ik},\chi_{jk}\}$ manifolds, respectively, and appropriate replacement equations[99,100] must be invoked to deperturb the anharmonic constants of these interactions, as signified by the asterisks appearing in the above summations. In Table VI each occurrence of an asterisk correspondingly denotes the removal of a particular resonance term in deperturbing a χ_{ij} value, and accompanying entries in brackets reveal the quantitative effects of these resonances, which are explicitly identified and properly treated in Sec. VI.

The diagonal anharmonic constants for the stretching modes of both H_2CCO and D_2CCO are comprised of negative cubic terms compensated by positive quartic contributions smaller in magnitude by roughly a factor of 2, a typical balance for strong chemical bonds. In contrast, for the group B modes (5,6,9) involving substantial C═C═O deformation, Σ_1 either cancels or actually supersedes Σ_2. The case of $\chi_{66}(H_2CCO)$ is most conspicuous—the quartic term engenders an unusually large constant greater than 14 cm^{-1} regardless of whether the (ω_4,$2\omega_6$) resonance interaction is included. Nevertheless, both χ_{55} and χ_{99} of the parent isotopomer are less than +0.7 cm^{-1}, but in the former instance only because the (ω_4,$2\omega_5$) interaction is excluded. Since perdeuteration unmixes the (ω_5,ω_6) pair, the behavior of χ_{55} and χ_{66} for D_2CCO is intermediate between the extremes observed for H_2CCO. There are five constants for the two isotopomers for which the Σ_3 contribution greatly exceeds 5 cm^{-1}. Each case entails an interaction of a (b_1,b_2) pair of modes via the $A_e\hat{p}_a^2$ term in the J=0 Hamiltonian involving the vibrational angular momentum component $\hat{p}_a=\Sigma_{ij}\zeta_{ij}^a\hat{Q}_i\hat{P}_j$ about the molecular a axis.[96] It is clearly the magnitude of the A_e rotational constants of H_2CCO (9.5 cm^{-1}) and D_2CCO (4.7 cm^{-1}) which engenders the large Coriolis effects. Finally, by successive recomputations of the

TABLE VII. Summary of final vibrational analysis for H_2CCO, HDCCO, and D_2CCO.[a]

Mode	Description	ω	Δ_{Anh}	Δ_{Res}	Δ_{Cor}	ν	Expt.[b]	IR intensity[c]	TED[d]
H_2CCO									
ν_1 (a_1)	C–H sym. str.	3202.2	−129.3	−1.0	1.1	3073.0	3070.4	32.0	$S_1(99)$
ν_2	C=O (asym.) str.	2197.2	−45.9	0	1.5	2152.8	2152.6	529.3	$S_2(70)-S_4(30)$
ν_3	CH_2 scissor	1415.2	−25.3	−1.4	0.8	1389.3	1386.6[e]	17.2	$S_3(83)-S_4(12)-S_2(5)$
ν_4	C=C (sym.) str.	1146.0	−17.7	−12.1	0.1	1116.3	(1116.0)	0.8	$S_4(58)+S_2(25)+S_3(17)$
ν_5 (b_1)	CH_2 wag	581.9	−11.5	0	18.6	589.0	587.3	42.8	$S_6(58)+S_5(42)$
ν_6	C=C=O linear bend	502.6	7.8	0	18.5	528.9	528.4	88.5	$S_5(58)-S_6(42)$
ν_7 (b_2)	C–H asym. str.	3308.2	−172.7	8.4	23.0	3166.9	3165.4[e]	11.4	$S_7(100)$
ν_8	CH_2 rock	996.0	−24.5	0	6.6	978.1	977.8	3.5	$S_8(78)+S_9(22)$
ν_9	C=C=O linear bend	433.6	−3.0	0	8.0	438.6	439.0	2.4	$S_9(78)-S_8(22)$
HDCCO									
ν_1 (a')	C–D str.	2398.8	−81.1	−4.3	4.4	2317.8	2318.9	64.7	$S_1(53)-S_7(41)-S_4(4)$
ν_2	C=O (asym.) str.	2187.9	−45.2	0	1.5	2144.2	2142.4	484.2	$S_2(69)-S_4(26)$
ν_3	CHD scissor	1315.1	−24.9	0	0.7	1290.9	1292	11.2	$S_3(58)-S_4(27)-S_2(11)$
ν_4	C=C (sym.) str.	1107.6	−20.6	−10.0	0.9	1077.9	(1084.9)	2.1	$S_4(40)+S_3(29)+S_2(17)+S_8(12)$
ν_5 (a'')	C=C=O linear bend	547.7	−3.9	0	9.3	553.1	555.3	7.5	$S_5(85)+S_6(15)$
ν_6	CHD wag	476.4	3.7	0	17.0	497.1	496.8	98.2	$S_6(85)-S_5(15)$
ν_7 (a')	C–H str.	3259.3	−154.5	0	12.9	3117.7	3117.3	20.0	$S_7(57)+S_1(43)$
ν_8	CHD rock	878.6	−24.7	0	4.4	858.3	(867.1)	3.8	$S_8(54)+S_9(29)-S_3(13)$
ν_9	C=C=O linear bend	396.7	−3.1	0	5.0	398.6	397.6	2.1	$S_9(68)-S_8(31)$
D_2CCO									
ν_1 (a_1)	C–D sym. str.	2345.5	−79.9	0	0.9	2266.5	2267.3	152.6	$S_1(83)-S_4(10)+S_2(6)$
ν_2	C=O (asym.) str.	2173.0	−44.0	[−12.2][f]	1.4	2118.2	2120.5	405.6	$S_2(65)-S_4(21)-S_1(14)$
ν_3	C=C (sym.) str.	1239.2	−19.3	4.8	0.3	1225.0	1225	4.6	$S_4(53)-S_3(23)+S_2(22)$
ν_4	CD_2 scissor	925.5	−16.2	12.2	0.4	921.9	924.7	4.7	$S_3(77)+S_4(16)+S_2(7)$
ν_5 (b_1)	C=C=O linear bend	533.8	2.3	0	5.9	542.0	541.2	0.5	$S_5(103)$
ν_6	CD_2 wag	421.5	−0.8	0	13.0	433.7	434.7	79.6	$S_6(103)$
ν_7 (b_2)	C–D asym. str.	2466.0	−96.8	0	11.7	2380.9	2383.3	6.8	$S_7(100)$
ν_8	CD_2 rock	861.9	−15.2	0	3.9	850.6	851.7	3.7	$S_8(63)+S_9(37)$
ν_9	C=C=O linear bend	370.7	−3.0	0	3.7	371.4	371.6[g]	1.9	$S_9(63)-S_8(37)$

[a]QZ($2d,2p$) SQM(CCSD)+MP2//EXPT values (in cm^{-1}) are given for the harmonic frequencies (ω_i), anharmonicity components (Δ_i), and fundamental vibrational frequencies (ν_i). Δ_{Anh} is the principal component of the fundamental frequency arising from the anharmonicity of the potential energy surface, while Δ_{Cor} and Δ_{Res} are additional contributions due to Coriolis effects and specific vibrational resonances, respectively.

[b]Empirical fundamental frequencies, as collected in Ref. 28, unless otherwise noted. Questionable assignments appear in parentheses.

[c]Theoretical infrared intensities (km mol^{-1}) within the double-harmonic approximation based on the unscaled QZ($2d,2p$) MP2 quadratic force constants and dipole-moment derivatives.

[d]The percentage proportions k of the total energy (kinetic and potential) of each normal vibration attributable to the individual internal coordinates S_i are indicated as $S_i(k)$ entries (see Ref. 89). The signs preceding these entries denote the relative phases of the internal coordinates in the normal-mode eigenvectors. The phases for HDCCO correspond to deuteration at position H_4 in Fig. 2.

[e]The ν_3 and ν_7 frequencies of CH_2CO are resonance-perturbed values from Refs. 27 and 26, respectively.

[f]The combination band $\nu_3+\nu_4=2158.6$ cm^{-1} observed by Moore and Pimentel (Ref. 17) is utilized in this case to ascertain the magnitude of the resonance splitting.

[g]Reference 30.

χ_{ij} constants, it is possible to identify a set of internal force field elements which negligibly affect the anharmonic vibrational analysis. Adopting the criterion that the F_{ijk} and F_{ijkl} values included in the set must individually and *collectively* alter no anharmonic constant by more than 0.25 cm^{-1}, the elements labeled by asterisks in Tables IV and V are identified. In brief, it appears that 18 of 56 cubic and 76 of 163 quartic constants can be eliminated with minimal consequences in future vibrational studies of ketene.

A summary of the final vibrational analysis of ketene isotopomers is presented in Table VII, which lists mode assignments, harmonic and fundamental frequencies, anharmonicity components, infrared intensities, and total energy distributions (TEDs). The summary data show that the fundamental frequencies of the modes included in the SQM refinement are reproduced to within 2.8 cm^{-1} in all cases, the average absolute deviation being a mere 1.1 cm^{-1}. Much larger residuals of 7.0 and 8.8 cm^{-1}, respectively, are found for ν_4 and ν_8 of HDCCO, revealing the dubiosity of these assignments and the need for an improved experimental analysis of these bands. Each total anharmonicity ($\Delta_i \equiv \nu_i - \omega_i$) in Table VII is partitioned into the principal anharmonic term (Δ_{Anh}) arising from the $\Sigma_1+\Sigma_2$ component of the χ_{ij} constants, the Coriolis contribution (Δ_{Cor}) given by corresponding Σ_3 quantities, and in cases a resonance splitting explicitly determined by a first-order treatment (Sec. VI). For $\nu_7(H_2CCO)$, $\nu_2(D_2CCO)$, and ν_4 of each species, a $|\Delta_{Res}|$ value exceeding 8 cm^{-1} is observed, demonstrating the importance of resonance interactions in the vibrational treatment, notwithstanding the greater chemical significance attributable to the total anharmonicities ($\Delta^* = \Delta_{Anh}+\Delta_{Cor}$) of the unperturbed fundamentals. Some features of the TEDs were mentioned previously, viz., variations upon deuteration of the (S_5,S_6) mixing in (ω_5,ω_6) and the noticeable (S_1,S_2) mixing in (ω_1,ω_2) of D_2CCO; relevant aspects of the IR in-

TABLE VIII. Carbon-13 isotopic shifts (cm^{-1}) of ketene fundamentals.[a]

	$H_2{}^{13}CCO$			$H_2C^{13}CO$		
	$\Delta\omega$	$\Delta\nu$	Obs.	$\Delta\omega$	$\Delta\nu$	Obs.
ν_1 (a_1)	−5.82	−5.76[b]	−5.6	−0.05	−0.28[b]	−0.1
ν_2	−5.30	−6.02	−5.4[c]	−59.76	−56.52	−56.6
ν_3	−13.57	−12.21*	−12.4*	−0.02	−0.25*	···
ν_4	−16.48	−15.51*	···	−0.86	−0.83*	···
ν_5 (b_1)	−0.34	−0.44	−0.4	−6.06	−5.30	−5.4
ν_6	−5.68	−5.78	−5.5	−8.90	−9.97	−9.7
ν_7 (b_2)	−13.86	−13.55[d]	−13.8[d]	0.00	−5.10[d]	−4.2[d]
ν_8	−8.07	−7.76	−7.8	−10.24	−10.24	−10.4
ν_9	−0.08	−0.02	···	−7.74	−7.47	···

[a]The $\Delta\omega$ and $\Delta\nu$ isotopic shifts are derived from the QZ($2d,2p$) SQM(CCSD)+MP2//EXPT quartic force field; asterisks denote deperturbed quantities. The observed shifts in the empirical fundamentals result from the recent high-resolution spectroscopic analyses of Duncan and collaborators (Refs. 26–28).
[b]Including the ($\nu_1,\nu_4+2\nu_8$) resonance interaction gives −4.49 and +1.21 cm^{-1} for $H_2{}^{13}CCO$ and $H_2C^{13}CO$, respectively.
[c]Estimated in Ref. 27 by visual inspection of the spectrum.
[d]The corresponding deperturbed ν_7 shifts are ($\Delta\nu^*$, obs.)=(−12.31,−13.6) and (0.00, 0.0) cm^{-1} for $H_2{}^{13}CCO$ and $H_2C^{13}CO$, respectively.

tensity and TED data for the (ω_3,ω_4) series are considered in Sec. VI.

For the group A modes (1,2,3,4,7,8) of ketene, the Δ_i^* anharmonicities lie well within the corresponding ranges observed for carbon dioxide, ethylene, and formaldehyde. For example, the C═C═O stretching vibrations of H_2CCO exhibit the anharmonicities $\Delta_2^*=-44.4$ and $\Delta_4^*=-17.6$ cm^{-1}, whereas for CO_2 the corresponding (empirical) values[138] are −47.2 and −20.7 cm^{-1}, in order. Likewise, $\Delta_3^* = -24.5$ and $\Delta_8^* = -17.9$ cm^{-1} of H_2CCO correlate well with the anharmonicities of the a_g CH_2 scissor ($\Delta_3=-22.1$ cm^{-1}) and b_{1g} CH_2 rock ($\Delta_6=-20.1$ cm^{-1}) in ethylene, as evaluated at the DZP RHF//DZP RHF level of theory.[99] At variance with the ordinary anharmonic characteristics of their complementary modes, the group B vibrations (5,6,9) exhibit an intricate interplay of Δ_{Anh} and Δ_{Cor} effects. According to the TED analysis, the normal coordinates for ω_5 and ω_6 transform smoothly upon successive deuteration from roughly equal *cis* and *trans* mixtures of the two b_1 components to essentially pure C═C═O bend and CH_2 wag vibrations, respectively. Since the degree of C═C═O bending in each normal mode evidently determines the relative extent of positive anharmonicity, contravariant ascending and descending (H_2CCO, $HDCCO$, D_2CCO) series of Δ_{Anh} values result for the two b_1 vibrations: $\Delta_{\mathrm{Anh},5}=(-11.5, -3.9, +2.3)$ and $\Delta_{\mathrm{Anh},6}=(+7.8, +3.7, -0.8)$ cm^{-1}. Concurrently, the corresponding Δ_{Cor} quantities form decreasing sequences, $\Delta_{\mathrm{Cor},5}=(+18.6, +9.3, +5.9)$ and $\Delta_{\mathrm{Cor},6}=(+18.5, +17.0, +13.0)$ cm^{-1}, because the A_e molecular rotational constant diminishes upon deuteration. The preponderance of the Coriolis terms yields the total anharmonicity series $\Delta_5=(+7.1, +5.4, +8.2)$ and $\Delta_6=(+26.3, +20.7, +13.2)$ cm^{-1}, in which only positive values appear. Clearly the source of the large positive anharmonicity predicted for $\nu_6(H_2CCO)$ is a propitious superposition of Δ_{Anh} and Δ_{Cor} effects. For the b_2 C═C═O bend (ω_9), which involves significant *trans* coupling with the methylene rock, the character of the normal vibration is changed much less by deuteration than in the ω_5 and ω_6 examples. As a consequence, all $\Delta_{\mathrm{Anh},9}$ values lie near -3 cm^{-1}, resulting in a series of positive total anharmonicities, $\Delta_9=(+5.0, +1.9, +0.7)$ cm^{-1}, of limited magnitude with variations governed by the underlying Coriolis terms.

The carbon-13 isotopic shifts of the fundamental frequencies of H_2CCO derived from the QZ($2d,2p$) SQM(CCSD)+MP2//EXPT quartic force field are listed in Table VIII and compared to experimental observations.[26–28] Only the C═O stretching (ν_2) and CH_2 rocking (ν_8) fundamentals of $H_2C^{13}CO$ were included in the SQM refinement of the quadratic force field, the reproduction of the corresponding empirical frequencies being better than 0.5 cm^{-1} in both instances. Therefore, the excellent agreement between the observed and computed isotopic shifts over the entire data set in Table VIII provides independent confirmation of the anharmonic force field. Carbon-13 shifts of band systems ascribed to the C═C stretching fundamental (ν_4) have been observed[27] but are not listed in Table VIII because the analysis of the (ν_4, $2\nu_5$, $2\nu_6$, $\nu_5+\nu_6$) Fermi tetrad in Sec. VI reveals perplexing inconsistencies in the experimental assignments. The anharmonic contribution to the vibrational shifts of the carbon-13 isotopomers exceeds 0.5 cm^{-1} only for (ν_2, ν_3, ν_4) of $H_2{}^{13}CCO$ and (ν_2, ν_5, ν_6, ν_7) of $H_2C^{13}CO$. For each of the $H_2C^{13}CO$ shifts in this set, the anharmonic term brings the computed and observed values into strikingly better agreement. Only for $\nu_2(H_2{}^{13}CCO)$ is a marginal deterioration found, but this occurrence is almost certainly a consequence of the confused structure encountered in experimental work on the band system of this isotopomer, which precluded detailed assignments and necessitated visual estimation of the band origin.[27] The anharmonic effects on $\nu_7(H_2C^{13}CO)$ are particularly notable in that both the harmonic frequency and the deperturbed fundamental exhibit carbon-13 shifts of less than 0.01 cm^{-1}, while the observed shift[26] of -4.2 cm^{-1} is accounted for nicely by the isotopic variation of the computed resonance splitting within the (ν_7, $\nu_2+\nu_8$) doublet (see Sec. VI).

VI. VIBRATIONAL RESONANCES

In Table IX the resonance manifolds in H_2CCO, $HDCCO$, and D_2CCO are identified from which significant

TABLE IX. Vibrational resonance interactions for isotopomers of ketene.[a]

Resonance		Δ_{Res}	$E_{\pm}-E_{\pm}^{0}=\Delta_{Res}=-W^2/\Lambda$ W	Λ
H_2CCO	$(\nu_1,\ \nu_4+2\nu_8)$	−0.98	$\phi_{8841}/\sqrt{32}=2.69$	$\nu_4^*-\nu_1+2(\nu_8+\chi_{88}+\chi_{84})=7.4$
	$(\nu_3,\ \nu_8+\nu_9)$	−1.44	$\phi_{983}/\sqrt{8}=6.44$	$\nu_8+\nu_9-\nu_3+\chi_{98}^*=28.8$
	$(\nu_4,\ 2\nu_5,\ 2\nu_6,\ \nu_5+\nu_6)$	−12.08	⋯	⋯
	$(\nu_7,\ \nu_2+\nu_8)$	+8.37	$\phi_{872}/\sqrt{8}=17.90$	$\nu_2+\nu_8-\nu_7+\chi_{82}^*=-38.3$
HDCCO	$(\nu_1,\ \nu_3+\nu_4)$	−4.30	$\phi_{431}/\sqrt{8}=-15.46$	$\nu_3+\nu_4^*-\nu_1+\chi_{43}^*=55.6$
	$(\nu_4,\ 2\nu_5,\ 2\nu_6,\ \nu_5+\nu_6)$	−10.03	⋯	⋯
D_2CCO	$(\nu_2,\ \nu_3+\nu_4)$[b]	−12.22	$\phi_{432}/\sqrt{8}=17.78$	$\alpha W/(1-\sqrt{1-\alpha^2})=25.9$
	$(\nu_3,\ \nu_8+\nu_9)$	+4.84	$\phi_{983}/\sqrt{8}=3.99$	$\nu_8+\nu_9-\nu_3+\chi_{98}^*=-3.3$
	$(\nu_4,\ 2\nu_5,\ 2\nu_6,\ \nu_5+\nu_6)$	+12.23	⋯	⋯

[a]All values in cm^{-1}.
[b]$\alpha\equiv(\phi_{432}/\sqrt{2})[(\nu_3+\nu_4)-\nu_2]^{-1}=0.9335$.

perturbations of fundamental levels originate. The candidate $(\nu_2,2\nu_4)$ interaction of HDCCO was excluded from the set because it perturbs the C═O stretching fundamental (ν_2) by only 0.3 cm^{-1}, a value reproduced almost exactly by inclusion of the $(\omega_2,2\omega_4)$ terms for the relevant χ_{ij} constants. Apart from the $(\nu_4,\ 2\nu_5,\ 2\nu_6,\ \nu_5+\nu_6)$ Fermi tetrads for the three isotopomers, the identified resonances involve only two interacting states, and the corresponding splittings (Δ_{Res}) of the upper and lower unperturbed levels $(E_{\pm}^0)$ caused by the coupling matrix elements (W) within the 2×2 secular equation can be expressed as

$$\Delta_{Res}=E_{\pm}-E_{\pm}^0=-W^2/(E_{\mp}^0-E_{\pm}), \tag{11}$$

where $E_{\pm}$ denotes the final, perturbed levels. Except in the D_2CCO $(\nu_2,\nu_3+\nu_4)$ case, the separation parameters $\Lambda=E_{\mp}^0-E_{\pm}$ for the $(\nu_i,\nu_j+n\nu_k)$ resonances were computed as $\nu_j+n\nu_k-\nu_i+\lambda_{Anh}$ using empirical fundamental frequencies for all (ν_i,ν_j,ν_k) quantities, less ν_4^*, and theoretical λ_{Anh} anharmonic corrections from the deperturbed χ_{ij} values derived in this study. The deperturbed ν_4^* frequencies were taken from the Fermi tetrad analysis described below (see Table X). For all resonances, values of W were obtained by the analytic reduction of matrix elements of the connecting anharmonic terms in the QZ$(2d,2p)$ SQM(CCSD) +MP2//EXPT force field within the normal mode approximation for the interacting vibrational states. Some comparisons are possible of the quantities thus computed with effective W parameters deduced by empirical deperturbation analyses of ketene fundamentals. Notably, the W entries in Table IX for the $(\nu_3,\ \nu_8+\nu_9)$ and $(\nu_7,\ \nu_2+\nu_8)$ interactions of the parent isotopomer, 6.4 and 17.9 cm^{-1}, respectively, are in excellent agreement with the analogous empirical parameters $W_{983}\approx5.0$ and $W_{872}=16.0$ cm^{-1}.[26,27]

The principal merit of Eq. (11) is that it determines Δ_{Res} from related empirical fundamental levels and complementary theoretical data alone, i.e., the spectroscopic band origin of the perturbed combination level $\nu_j+n\nu_k$ is not required. However, for D_2CCO the collective uncertainty involved in

TABLE X. Data for ν_4 Fermi resonance tetrad of isotopomers of ketene.[a]

	H_2CCO	$H_2{}^{13}CCO$	$H_2C^{13}CO$	HDCCO	D_2CCO
ν_4^*	$w=1128.1$	$w-15.5$	$w-0.8$	$w-40.5$	$u=912.5$
$(2\nu_5)^*$	$x=1173.2$	$x-1.8$	$x-10.3$	1116.2	1088.2
$(2\nu_6)^*$	$y=1067.0$	$y-11.0$	$y-20.9$	1006.1	$v=879.9$
$(\nu_5+\nu_6)^*$	$z=1120.7$	$z-6.3$	$z-14.0$	1052.6	977.7
ϕ_{554}	120.91	110.34	118.37	105.01	35.04
ϕ_{664}	56.36	52.62	55.51	46.94	117.08
ϕ_{654}	2.52	10.02	6.96	34.28	52.14
χ_{55}^*	0.28	−0.21	0.55	2.78	2.92
χ_{66}^*	14.83	14.81	12.54	18.73	13.02
χ_{65}^*	14.92	13.81	18.28	1.56	5.30
λ_1[b]	1188.7 (1188.7)	1182.6 (1182.5)	1180.0 (1179.6)	1132.6	1088.7
λ_2	1120.8	1115.3	1113.4	1077.6	983.1
λ_3	1116.0 (1116.0)	1103.8	1106.0	1048.1	924.7 (924.7)
λ_4	1063.5 (1063.5)	1052.8 (1053.5)	1043.6 (1051.0)	1004.2	861.8 (861.8)
Ψ_1	$0.89\|020\rangle+0.46\|100\rangle$	$0.93\|020\rangle+0.37\|100\rangle$	$0.86\|020\rangle+0.50\|100\rangle$	$0.84\|020\rangle+0.53\|100\rangle$	$1.00\|020\rangle$
Ψ_2	$0.99\|011\rangle+0.14\|100\rangle$	$0.96\|011\rangle+0.25\|100\rangle$ $-0.12\|020\rangle$	$0.81\|100\rangle-0.48\|020\rangle$ $+0.17\|002\rangle+0.30\|011\rangle$	$0.76\|100\rangle-0.52\|020\rangle$ $+0.13\|002\rangle+0.37\|011\rangle$	$0.96\|011\rangle+0.28\|100\rangle$
Ψ_3	$0.85\|100\rangle-0.45\|020\rangle$ $+0.24\|002\rangle-0.16\|011\rangle$	$0.86\|100\rangle-0.35\|020\rangle$ $+0.24\|002\rangle-0.29\|011\rangle$	$0.95\|011\rangle-0.26\|100\rangle$ $+0.13\|020\rangle$	$0.92\|011\rangle-0.34\|100\rangle$ $+0.13\|020\rangle-0.10\|002\rangle$	$0.80\|100\rangle+0.52\|002\rangle$ $-0.28\|011\rangle$
Ψ_4	$0.97\|002\rangle-0.25\|100\rangle$	$0.97\|002\rangle-0.24\|100\rangle$	$0.98\|002\rangle-0.18\|100\rangle$	$0.99\|002\rangle-0.16\|100\rangle$	$0.85\|002\rangle-0.52\|100\rangle$

[a]All data for matrix elements and eigenvalues in cm^{-1}. See the text for details.
[b]Empirical values from Refs. 26, 27, and 30 in parentheses.

deperturbing both ν_3 and ν_4 renders Eq. (11) ineffective for the $(\nu_2,\nu_3+\nu_4)$ resonance. To circumvent this problem, the identity

$$E_{\pm}^{0}=\tfrac{1}{2}(E_{+}+E_{-})\pm\tfrac{1}{2}\sqrt{(E_{+}-E_{-})^{2}-4W^{2}} \tag{12}$$

was employed to obtain the seemingly recondite expression appearing as a special case for Λ in Table IX, the evaluation of which is made possible by an earlier spectroscopic observation[17] of a Q-branch center at 2158.6 cm^{-1} attributable to the perturbed $(\nu_3+\nu_4)$ combination level. The deperturbed C═O stretching fundamental for D_2CCO ascertained in this manner is fit consistently by the QZ($2d$,$2p$) SQM(CCSD)+MP2//EXPT quartic force field vis-à-vis the ν_2 band origins of H_2CCO, HDCCO, and $H_2C^{13}CO$, which do not suffer from resonance complications. Nevertheless, an improved experimental analysis of the $(\nu_3+\nu_4)$ band origin is warranted to fully dissect the $(\nu_2,\ \nu_3+\nu_4)$ manifold of D_2CCO.

The resonance interactions may be categorized as weak ($|\Delta_{Res}|<2$ cm^{-1}) for H_2CCO $(\nu_1,\nu_4+2\nu_8)$ and $(\nu_3,\nu_8+\nu_9)$, moderate ($2<|\Delta_{Res}|<6$ cm^{-1}) for HDCCO $(\nu_1,\nu_3+\nu_4)$ and D_2CCO $(\nu_3,\nu_8+\nu_9)$, and strong ($|\Delta_{Res}|>6$ cm^{-1}) for H_2CCO $(\nu_7,\nu_2+\nu_8)$, D_2CCO $(\nu_3,\nu_8+\nu_9)$, and the three Fermi tetrads. The $(\nu_1,\ \nu_4+2\nu_8)$ resonance has been suggested as the most probable source of observed Q-branch perturbations in the fundamental band system of the symmetric C–H stretching vibration in H_2CCO and its carbon-13 variants, even though the isotopic modulation and the K_a dependence of the interaction are not explained satisfactorily by this assignment alone.[27] The inclusion of the weak $(\nu_1,\nu_4+2\nu_8)$ resonance, which does not contribute to the second-order χ_{ij} constants, in the evaluation of the carbon-13 isotopic shifts of ν_1 actually spoils the excellent accord between theory and experiment evident in Table VIII (cf. footnote b therein). Consequently, the role of the $(\nu_1,\nu_4+2\nu_8)$ resonance must be questioned, although some of the observed deterioration may be fortuitous, since the $\nu_1(H_2CCO)$ band origin is not well defined.

Resonance effects for the $(\nu_3,\nu_8+\nu_9)$ manifold of H_2CCO and D_2CCO cannot be quantified experimentally to high accuracy due to the lack of assignable structure belonging to $\nu_8+\nu_9$. Nevertheless, acceptable explanations of Q-branch patterns observed among the H_2CCO, $H_2{}^{13}CCO$, and $H_2C^{13}CO$ species are possible,[27] and the aforementioned proximity of the effective W_{983} matrix elements extracted from the spectra to the values predicted here is compelling. For D_2CCO, the $(\nu_3,\ \nu_8+\nu_9)$ spectral region around 1227 cm^{-1} exhibits a highly compressed and confused structure, indicative of a ν_3 Fermi resonance with a slightly lower-lying vibration possessing a marked K_a degradation to lower frequency. Indeed, the data in Table IX predict a minuscule zeroth-order separation, $(\nu_8+\nu_9)^{*}-\nu_3^{*}=-\Lambda-\Delta_{Res}=-1.7$ cm^{-1}. The resulting resonance shift of 4.8 cm^{-1} is somewhat larger than the 2–3 cm^{-1} estimate of Duncan and co-workers.[27] In actuality, an intermediate value is likely, because the model 2×2 secular equation cannot give a resonance splitting larger than $W=4.0$ cm^{-1} if theoretical data are consistently used without intermingling experimental frequencies.

The $(\nu_4,2\nu_5,2\nu_6,\nu_5+\nu_6)$ Fermi tetrad of ketene isotopomers, a more intricate variant of the prototypical $(\nu_1,2\nu_2)$ stretch–bend resonance of CO_2, is responsible for a baffling set of spectroscopic observations which have heretofore eluded satisfactory explanation. The current analysis of this vibrational manifold is based on the model Hamiltonian

$$\mathbf{H}_{vib}=\begin{bmatrix} \nu_4^{*} & (\phi_{554}/4) & (\phi_{664}/4) & (\phi_{654}/\sqrt{8}) \\ (\phi_{554}/4) & (2\nu_5)^{*} & 0 & 0 \\ (\phi_{664}/4) & 0 & (2\nu_6)^{*} & 0 \\ (\phi_{654}/\sqrt{8}) & 0 & 0 & (\nu_5+\nu_6)^{*} \end{bmatrix}, \tag{13}$$

in which the unperturbed diagonal elements are adjusted to fit available experimental band origins with the aid of theoretical constraints, while the interaction matrix elements between the C═C (symmetric) stretching fundamental and the intermediate eigenstates for the bending overtone and combination levels are derived from the QZ($2d$,$2p$) SQM(CCSD)+MP2//EXPT anharmonic force field by a normal mode treatment, as before in Eq. (11).

In Table X a synopsis of the Fermi tetrad analysis for ketene isotopomers is presented. The tabulated λ_i entries are the eigenvalues of $\mathbf{H}_{vib}$, and the Ψ_i listings are the associated vibrational wave functions expressed in terms of the zeroth-order basis states $|v_4v_5v_6\rangle$. For H_2CCO the values of ν_4^{*}, $(2\nu_5)^{*}$, and $(2\nu_6)^{*}$ which reproduce the empirical band origins[26,27] $(\nu_4,2\nu_5,2\nu_6)=(1116.0,\ 1188.7,\ 1063.5)$ cm^{-1} are $(w,x,y)=(1128.1,\ 1173.2,\ 1067.0)$ cm^{-1}. Based on the formula $(2\nu_i)^{*}=2(\nu_i+\chi_{ii}^{*})$, the results for x and y correspond to the effective anharmonic constants $\chi_{55}^{*}=-0.7$ and $\chi_{66}^{*}=+5.1$ cm^{-1}. It is thus necessary to scale the χ_{66}^{*} constant (14.92 cm^{-1}) computed from the QZ($2d$,$2p$) SQM(CCSD)+MP2//EXPT force field by roughly (1/3) to obtain from second-order perturbation theory a $(2\nu_6)^{*}$ overtone positioned at y. The resolution of this enigma must be held in abeyance until further research is possible. For the present purpose of fixing for the various isotopomers those diagonal matrix elements of the Fermi tetrad which are empirically undetermined, the scale factor $\eta=(1/3)$ is assumed for χ_{66}^{*} and the related, large positive constant χ_{65}^{*} whenever second-order perturbation theory is invoked, all the while leaving χ_{55}^{*} unaltered. Accordingly, the parameter $z=1120.7$ cm^{-1} for H_2CCO was derived from the condition $(\nu_5+\nu_6)^{*}=\nu_5+\nu_6+\eta\chi_{65}^{*}$, with ν_5 and ν_6 taken from experiment.

The wave function (Ψ_3) from the tetrad model for the ν_4 fundamental level of H_2CCO at 1116 cm^{-1} is a strong admixture containing 72% $|1\ 0\ 0\rangle$, 20% $|0\ 2\ 0\rangle$, 6% $|0\ 0\ 2\rangle$, and 2% $|0\ 1\ 1\rangle$. Another eigenstate lying less than 5 cm^{-1} higher is almost exclusively $|0\ 1\ 1\rangle$. Duncan and Ferguson[26] have raised the possibility that the absorption band in this spectral region is more correctly described as $\nu_5+\nu_6$ and that ν_4 is too weak to be observed. The data in Table VII reveal that ν_4, whose IR intensity is only 0.8 km mol^{-1}, is indeed the weakest fundamental of H_2CCO, but only by a factor of 3 relative to the observable ν_9 band. A definitive resolution of this issue awaits a theoretical evaluation of the anharmonic transition dipole moment for the $\nu_5+\nu_6$ absorption. However, the

placement of $\nu_4(H_2CCO)$ *near* 1116 cm^{-1} is confirmed through the present vibrational analysis on the basis of the compelling consistency among the ν_3 and ν_4 fundamental assignments of H_2CCO and D_2CCO. This validation is not specious, because the character of normal modes 3 and 4 is dramatically transformed upon deuteration, as documented by the TED elements in Table VII. To wit, the normal vibration associated with $\nu_3(D_2CCO)$ at 1225 cm^{-1} is 53% S_4(C═C stretch), 23% S_3(methylene scissor), and 22% S_2(C═O stretch), exhibiting almost the same components as the *lower* frequency $\nu_4(H_2CCO)$, except that the phase of S_3 mixing is inverted. Conversely, $\nu_4(D_2CCO)$ at 925 cm^{-1} is predominantly a methylene scissoring mode with a total energy distribution very similar to that of $\nu_3(H_2CCO)$. In brief, for each isotopomer the deperturbed ν_4^* fundamental reconstructed from the large resonance shift ($\Delta_{Res}=\pm 12$ cm^{-1}) given by the Fermi tetrad analysis is cross-checked in the overall vibrational procedure by a corresponding ν_3^* fundamental for the other species extracted from the $(\nu_3,\nu_8+\nu_9)$ manifold, for which resonance effects are much less severe.

The location of $\nu_4^*(H_2CCO)$ can actually be deduced without relying on the questionable experimental assignments for the perturbed ν_4 fundamentals of ketene isotopomers. The Ψ_1 vibrational wave functions in Table X are comprised solely of $|0\ 2\ 0\rangle$ and $|1\ 0\ 0\rangle$ for all intents and purposes. The carbon-13 isotopic modulation of the $2\nu_5$ overtone can thus be analyzed via a two-state model for the perturbation arising from ν_4. By applying Eq. (11) to the $(2\nu_5,\nu_4)$ interaction for isotopomers $A=H_2CCO$ and $B=H_2{}^{13}CCO$ and then subtracting the resulting expressions, the isotopic shift in $2\nu_5$ is related to the extent of separation within the resonance pairs. Specifically,

$$\delta_a-\delta_b=\frac{W_A^2}{(2\nu_5)_A-(\nu_4^*)_A}-\frac{W_B^2}{(2\nu_5)_B-(\nu_4^*)_B}, \tag{14}$$

in which $\delta_a=[(2\nu_5)_A-(2\nu_5)_B]$ and $\delta_b=[(2\nu_5)_A^*-(2\nu_5)_B^*]$. The spectroscopically determined δ_a shift is 6.2 cm^{-1},[27] whereas the unperturbed δ_b quantity is 1.8 cm^{-1} and the relevant matrix elements are $W_A=30.23$ and $W_B=27.58$ cm^{-1}, according to the QZ$(2d,2p)$ SQM(CCSD)+MP2// EXPT anharmonic force field. Moreover, the ν_4^* isotopic shift predicted by this force field is 15.51 cm^{-1} (Table VIII), whose substitution into Eq. (14) yields a quadratic form for the unknown quantity $\lambda=(\nu_4^*)_A$; namely,

$$t=\frac{W_A^2}{r-\lambda}-\frac{W_B^2}{s-\lambda}, \tag{15}$$

where $t=\delta_a-\delta_b=4.4$, $r=(2\nu_5)_A=1188.7$, and $s=(2\nu_5)_B+\delta_b=1198.0$ cm^{-1}. The nonextraneous solution to Eq. (15) is $\lambda=\nu_4^*(H_2CCO)=1130.2$ cm^{-1}, in remarkable agreement with the 1128.1 cm^{-1} value derived from the Fermi tetrad analysis.

For D_2CCO the observed band origins[27,30] $\nu_4=924.7$ and $2\nu_6=861.8$ cm^{-1} are fit by the unperturbed quantities $u=(2\nu_5)^*=912.5$ and $v=(2\nu_6)^*=879.9$ cm^{-1}, assuming the other diagonal matrix elements are evaluated from perturbation theory. The effective χ_{66}^* constant corresponding to the $(2\nu_6)^*$ level is a factor of 2.5 smaller than the computed value (+13.0 cm^{-1}) listed in Tables VI and X, a disparity similar to that occurring for the parent species. The λ_1 and λ_2 levels for D_2CCO are essentially pure $|0\ 2\ 0\rangle$ and $|0\ 1\ 1\rangle$ eigenstates, respectively, and the primary mixing now occurs between $|1\ 0\ 0\rangle$ and $|0\ 0\ 2\rangle$ in λ_3 and λ_4. Because the separation of λ_2 and λ_3 increases upon perdeuteration from 5 to 58 cm^{-1}, the assignment of the band system in the intermediate region of the tetrad is no longer ambiguous.

For HDCCO, $H_2{}^{13}CCO$, and $H_2C^{13}CO$, all diagonal elements of $\mathbf{H}_{vib}$ were fixed by theoretical considerations, and thus the solutions of the Fermi tetrad analysis are independent predictions to elucidate the spectral features of this vibrational manifold. As before, the unperturbed bending levels were determined from $(2\nu_5)^*=2(\nu_5)+2\chi_{55}^*$, $(2\nu_6)^*=2(\nu_6)+2\eta\chi_{66}^*$, and $(\nu_5+\nu_6)^*=\nu_5+\nu_6+\eta\chi_{65}^*$ with empirical ν_5 and ν_6 fundamentals. Concomitantly the unperturbed stretching levels were ascertained from computed isotopic shifts in ν_4^* relative to the value $w=1128.1$ cm^{-1} found in the parent (cf. Tables VII, VIII, and IX).

The HDCCO species exhibits the most severe mixing of basis states among the λ_1 and λ_2 levels of the ketene isotopomers. In fact, the wave function (Ψ_2) assignable to the C═C symmetric stretch (1078 cm^{-1}) is only 58% $|1\ 0\ 0\rangle$. The experimental result (1085 cm^{-1}) for $\nu_4(HDCCO)$ cannot be accounted for by allowing the ν_4^* and $(2\nu_5)^*$ parameters to vary within reasonable limits from the fixed values given in Table X. Accordingly, the 7 cm^{-1} discrepancy for ν_4 casts doubt on the spectral assignments in this region, as mentioned in Sec. V.

The empirical carbon-13 shifts for the Fermi tetrad levels are ''at complete variance with expectation,'' to quote the spectroscopic work of Duncan *et al.*,[27] whose assessment is corroborated by the current analysis. The observed ($H_2{}^{13}CCO$, $H_2C^{13}CO$) shifts for ν_4 are (−5.2,−7.9) cm^{-1}, in striking discord with the (−12.2,−2.6) cm^{-1} values predicted here. Note that the compositions of the vibrational wave functions for the (λ_2,λ_3) levels of $H_2C^{13}CO$ are inverted relative to $H_2{}^{13}CCO$, but the degree of $|1\ 0\ 0\rangle$ and $|0\ 1\ 1\rangle$ mixing is modest in both cases. The QZ$(2d,2p)$ MP2 infrared intensities for ν_4 in the double-harmonic approximation are 0.3 and 0.6 km mol^{-1} for $H_2{}^{13}CCO$ and $H_2C^{13}CO$, respectively, i.e., even smaller than that for the parent isotopomer (cf. Table VII). Reassignment of the observed bands to the $\nu_5+\nu_6$ level is thus plausible. However, the predicted ($H_2{}^{13}CCO$, $H_2C^{13}CO$) isotopic shifts for $\nu_5+\nu_6$ are (−5.5, −14.8) cm^{-1}, in agreement with experiment in the first but not the second case. As for HDCCO, the disparities with the observed ν_4 shifts cannot be resolved by credible choices of the diagonal parameters in $\mathbf{H}_{vib}$. It is apparent that a satisfactory interpretation of the morass exhibited by the carbon-13 isotopomers in the 1100 cm^{-1} spectral region remains elusive.

VII. OVERTONE AND COMBINATION LEVELS

Apart from the fundamental levels of ketene, the excited vibrational states which have been subjected to detailed band analyses by means of high-resolution spectroscopy are severely limited in number. Therefore, the overtone and com-

TABLE XI. Selected overtone and combination levels of H_2CCO.[a]

Level	Experiment Ref.	Experiment ν_0	Theory Direct	Theory Adjusted
$2\nu_8$	27	1952.4 ($\chi_{88}=-1.56$)	1952.5 ($\chi_{88}=-1.83$)	1951.9
$\nu_3+\nu_4$	13	2513.6 ($\chi_{43}=-2.5$)	2516.2 ($\chi_{43}=-2.88$)	2513.2
$(\nu_2+\nu_8)^*$	26	3126.7 ($\chi^*_{82}=-3.7$)	3127.6 ($\chi^*_{82}=-3.28$)	3127.1
$\nu_2+\nu_4$	12	3266 ($\chi_{42}=-14.7$)	3267.2 ($\chi_{42}=-13.97$)	3266.7
$\nu_1+\nu_7$	13	6113.3 ($\chi_{71}=-115.1$)	6120.2 ($\chi_{71}=-112.25$)	6116.2

[a]All band origins and anharmonic constants in cm^{-1}.

bination bands predicted by the QZ($2d,2p$) SQM(CCSD) +MP2//EXPT anharmonic force field can only be assessed by sporadic comparisons with experimental data of varying quality reported in the literature since 1950. In Table XI theoretical and empirical data are presented for selected energy levels of H_2CCO lying above 1900 cm^{-1}. Despite the fact that three entries antedate 1960, the predicted and observed band origins are in excellent accord, especially if the direct theoretical results are adjusted by the residuals for reproducing the underlying ν_i quantities. For each experimental level in the table, an effective χ_{ij} constant is listed, as extracted from the relations $\chi_{ii}=\frac{1}{2}(2\nu_i)-\nu_i$ and $\chi_{ij}=(\nu_i+\nu_j)-\nu_i-\nu_j$, with the observed fundamentals deperturbed by the Δ_{Res} values in Table VII if necessary. The small χ_{88}, χ_{43}, and χ^*_{82} values agree with their theoretical counterparts to better than 0.5 cm^{-1}, whereas the larger χ_{42} and χ_{71} quantities differ from the predicted constants by only 5% and 2.5%, respectively. These comparisons redound to the veracity of the QZ($2d,2p$) SQM(CCSD)+MP2//EXPT force field, and in particular the deperturbed fundamental $\nu^*_4=1128$ cm^{-1} derived therefrom, since it nicely accounts for both $\nu_3+\nu_4$ and $\nu_2+\nu_4$. Additional low-resolution overtone and combination bands of H_2CCO above 1900 cm^{-1} are reported in the 1957 study of Arendale and Fletcher,[12] but all are devoid of detailed structure and some appear to be misassigned.

The overtone levels of ketene which have received the most spectroscopic attention are $2\nu_5$ and $2\nu_6$, which are involved in intricate Fermi resonance interactions with the ν_4 fundamental, as discussed extensively in Sec. VI. It was recognized even in the earliest studies[17] of the infrared spectrum of ketene that the positions of these overtones evidence abnormal anharmonicity for the b_1 bending fundamentals, a phenomenon borne out by the χ_{ij} constants of the current investigation. The *extent* of the positive anharmonicity displayed by these modes is the point of difficulty, however. While the observed $2\nu_5$ overtone of H_2CCO gives an effective χ_{55} value (-0.7 cm^{-1}) in reasonable proximity to the theoretical constant ($+0.28$ cm^{-1}), the empirical $2\nu_6$ level appears to require χ_{66} ($+5.1$ cm^{-1}) to be roughly 1/3 as large as the predicted result ($+14.83$ cm^{-1}), an enigma discovered in Sec. VI. Moreover, the observed carbon-13 shift in $2\nu_5$ is well described by the theoretical Fermi tetrad treatment in both the $H_2{}^{13}CCO$ and $H_2C^{13}CO$ cases, but only for $H_2{}^{13}CCO$ is the assigned $2\nu_6$ position explained even after scaling the χ_{66} constant (see Table X). In fact, both the $\nu_4=1108.1$ cm^{-1} and $2\nu_6=1051.0$ cm^{-1} experimental assignments[27] for $H_2C^{13}CO$ are at variance with the tetrad model results listed in Table X. As evident from the discussion in Sec. VI, both experimental and even higher-level theoretical reexaminations of the $2\nu_5$ and $2\nu_6$ overtones are warranted.

The $2\nu_9-\nu_9$, $\nu_6+\nu_9-\nu_9$, and $2\nu_6-\nu_6$ hot bands of D_2CCO were analyzed in the 1987 high-resolution work of Hegelund and co-workers,[30] whence $2\nu_9=743.33$, $\nu_6+\nu_9=807.24$, and $2\nu_6=861.82$ cm^{-1} were ascertained. The effective anharmonic constants resulting from the first two levels are $\chi_{99}=0.22$ and $\chi_{96}=0.96$ cm^{-1}, which compare rather poorly with the corresponding theoretical values ($\chi_{99}=0.66$ and $\chi_{96}=0.25$ cm^{-1}) appearing in Table VI. Difficulties appearing after deperturbation of the χ_{66} constant were mentioned in Sec. VI. Several low-resolution assignments for overtone and combination bands of D_2CCO appear in the 1963 study of Moore and Pimentel,[17] most being qualitatively correct but some quantitatively problematic vis-à-vis the set of anharmonic constants advanced here. Of significance to the resonance analyses of Sec. VI is the placement of $\nu_2+\nu_3$ and $\nu_2+\nu_4$ in the vicinity of 3338 and 3045 cm^{-1}, respectively. By comparison, the formula $(\nu_2+\nu_j)=\nu_2-\Delta_{\mathrm{Res},2}+\nu_j-\Delta_{\mathrm{Res},j}+\chi^*_{j2}$ predicts 3344 and 3042 cm^{-1}, in order, for $j=3$ and 4, based on empirical, perturbed fundamentals and theoretical anharmonic corrections. Despite the substantial uncertainty in the observed band origins, a broad level of agreement is thus seen which lends further support to the deperturbation treatments.

VIII. VIBRATION–ROTATION INTERACTION CONSTANTS

The QZ($2d,2p$) SQM(CCSD)+MP2//EXPT force field provides numerous heretofore unknown anharmonic spectroscopic quantities in addition to the χ_{ij} parameters, including the complete set of vibration–rotation interaction constants (α_i) listed in Table XII for H_2CCO and D_2CCO. The form of the standard expression[95,96] for these constants is

$$\alpha_i^B=-\left(\frac{2B_e^2}{\omega_i}\right)\left[\sum_\gamma \frac{3(a_i^{b\gamma})^2}{4I_{\gamma\gamma}}+\sum_j{}^* \frac{(\zeta_{ij}^b)^2(3\omega_i^2+\omega_j^2)}{\omega_i^2-\omega_j^2} + \pi\left(\frac{c}{h}\right)^{1/2}\sum_j \phi_{iij}a_j^{bb}\left(\frac{\omega_i}{\omega_j^{3/2}}\right)\right], \tag{16}$$

where $a_i^{\beta\gamma}\equiv(\partial I_{\beta\gamma}/\partial Q_i)_e$, and the asterisk on the second summation signifies the exclusion of the $i=j$ term. The three summations in Eq. (16) comprise, in order, the inertial-derivative, Coriolis, and anharmonic components of the vibration–rotation interaction constants, partitions which are included in the α_i listings of Table XII.

It is firmly documented that the (ν_5,ν_6,ν_8,ν_9) fundamentals of isotopic ketenes form a tetrad of strongly interacting, a-type Coriolis resonances.[23,24,30] Accordingly, detailed comparisons of theory and experiment require in cases the deperturbation of certain α_i values in Table XII, which as given

TABLE XII. Vibration–rotation interaction constants (α_i) for H_2CCO and D_2CCO.[a]

	H_2CCO				D_2CCO			
α_1^A	160.7	(−121.9,	0.0,	282.6)	65.9	(−32.0,	0.0,	98.0)
α_2^A	9.4	(−0.7,	0.0,	10.1)	6.5	(−7.0,	0.0,	13.5)
α_3^A	−128.8	(−95.6,	0.0,	−33.2)	−22.6	(−18.2,	0.0,	−4.4)
α_4^A	1.9	(−9.1,	0.0,	11.0)	−28.1	(−23.6,	0.0,	−4.5)
α_5^A	−1218.8	(0.0,	−1165.6,	−53.2)	−128.7	(0.0,	−125.7,	−3.0)
α_6^A	−442.1	(0.0,	−352.3,	−89.8)	−67.8	(0.0,	−14.0,	−53.9)
α_7^A	117.3	(−1.3,	−129.1,	247.8)	43.1	(−0.7,	−45.0,	88.7)
α_8^A	−514.7	(−9.1,	−410.3,	−95.3)	−199.6	(−3.4,	−175.1,	−21.1)
α_9^A	2125.4	(−12.4,	2246.7,	−108.8)	362.4	(−9.5,	418.8,	−46.9)
α_1^B	0.266	(0.0,	−0.063,	0.329)	0.592	(−0.001,	−0.110,	0.702)
α_2^B	2.515	(−0.006,	−0.343,	2.864)	1.818	(−0.004,	−0.243,	2.065)
α_3^B	−0.102	(−0.025,	−0.435,	0.359)	0.859	(−0.221,	−0.181	1.260)
α_4^B	0.714	(−0.577,	−0.046,	1.337)	−0.485	(−0.296,	−0.290,	0.101)
α_5^B	−0.098	(0.0,	0.632,	−0.730)	−0.169	(0.0,	0.463,	−0.631)
α_6^B	0.141	(0.0,	0.614,	−0.474)	0.023	(0.0,	0.681,	−0.659)
α_7^B	0.364	(−0.049,	0.0,	0.413)	0.511	(−0.044,	0.0,	0.555)
α_8^B	−0.507	(−0.330,	0.0,	−0.176)	−0.399	(−0.217,	0.0,	−0.181)
α_9^B	−1.452	(−0.452,	0.0,	−1.000)	−1.408	(−0.614,	0.0,	−0.795)
α_1^C	0.440	(−0.008,	−0.207,	0.654)	0.828	(−0.011,	−0.138,	0.978)
α_2^C	2.337	(−0.005,	−0.337,	2.679)	1.631	(0.0,	−0.241,	1.872)
α_3^C	0.513	(−0.046,	0.266,	0.293)	0.971	(−0.241,	0.116,	1.096)
α_4^C	0.622	(−0.490,	−0.147,	1.259)	−0.348	(−0.179,	−0.242,	0.073)
α_5^C	−0.745	(0.0,	0.0,	−0.745)	−0.568	(0.0,	0.0,	−0.568)
α_6^C	−0.552	(0.0,	0.0,	−0.552)	−0.778	(0.0,	0.0,	−0.778)
α_7^C	0.420	(0.0,	−0.270,	0.690)	0.472	(0.0,	−0.342,	0.814)
α_8^C	0.233	(0.0,	0.515,	−0.282)	0.463	(0.0,	0.700,	−0.237)
α_9^C	−0.488	(0.0,	0.577,	−1.065)	−0.377	(0.0,	0.496,	−0.872)

[a]Obtained from the QZ($2d,2p$) SQM(CCSD)+MP2//EXPT anharmonic force field. All constants are in units of 10^{-3} cm^{-1}. In parentheses the α_i constants are decomposed into inertial-derivative, Coriolis, and anharmonicity components, as defined in Eq. (16).

include all Coriolis interactions in the second-order expression [Eq. (16)]. Such deperturbations are readily accomplished using the ζ_{ij} constants collected in Table XIII below. The strong interactions within the (ν_5,ν_6,ν_8,ν_9) Coriolis tetrad manifest corresponding α_i^A constants for H_2CCO which are (12.9%, 4.7%, 5.4%, 22.5%) as large as the A_e rotational constant itself. The validity of the second-order perturbation formula [Eq. (16)] is thus suspect for this manifold, particularly for α_5^A and α_9^A, although the type of catastrophic breakdown observed for the quasilinear HNCO molecule[103] is clearly not operative. For D_2CCO the two largest a-axis parameters are α_9^A and α_8^A, which are only 7.6% and 4.2% of A_e, respectively, indicative of much more favorable circumstances for perturbation theory. In this regard it is auspicious that all α_i^B and α_i^C constants for both isotopomers are significantly less than 1% of the corresponding B_e and C_e values.

For the stretching modes of H_2CCO and D_2CCO, the anharmonic component of α_i is preponderate for every rotational constant, except in the two cases [$\alpha_4^A(H_2CCO)$ and $\alpha_3^A(D_2CCO)$] involving the effect of C═C (symmetric) stretching on I_A. Nevertheless, the Coriolis and inertial-derivative terms for such modes are large in several instances, e.g., α_1^C, α_7^A, α_1^A, and α_4^B of H_2CCO. For the vibrations involving substantial C═C═O bending [$H_2CCO(\nu_5,\nu_6,\nu_9)$, $D_2CCO(\nu_5,\nu_9)$], the α_i^A and α_i^C values are principally comprised, in order, of Coriolis and anharmonic terms, while their α_i^B counterparts have roughly equivalent contributions from both of these sources. The methylene scissoring and rocking modes engender two constants for each isotopomer, α_3^A and α_8^B, for which the inertial-derivative component is largest.

Several spectroscopic investigations[9,13,16,17,20,23] of ketene prior to 1986 determined rotational constants for excited vibrational states from which sporadic α_i values ensue. The level of accord with the current predictions is very good in some cases but generally mixed. More recent empirical vibration–rotation interaction parameters are provided by the 1987 work of Duncan and collaborators.[26,27] In units of 10^{-3} cm^{-1}, the negative differences of upper- and lower-state rotational constants observed for the a_1 fundamentals ν_1, ν_2, and ν_3 are $-(\Delta A_1,\Delta B_1,\Delta C_1)$=[158(25), 0.340(77), 0.418(74)], $-(\Delta A_2,\Delta B_2,\Delta C_2)$=[94(8), 2.58(5), 1.85(5)], and $-(\Delta A_3,\Delta B_3,\Delta C_3)$=[−140, −0.322(6), 0.476(6)], which are to be compared with the predicted values ($\alpha_1^A,\alpha_1^B,\alpha_1^C$)=(161, 0.266, 0.440), ($\alpha_2^A,\alpha_2^B,\alpha_2^C$)=(9.4, 2.52, 2.34), and ($\alpha_3^A,\alpha_3^B,\alpha_3^C$)=(−129, −0.102, 0.513). Considering both inherent experimental limitations and the expected accuracy of the theoretical methodology, the agreement is heartening in all cases except α_2^A and perhaps α_3^B. For the levels assigned to $\nu_4(H_2CCO)$, the empirical band analysis yields $-(\Delta A_4,\Delta B_4)$=(530, −0.313)×10^{-3} cm^{-1}, which bear little resemblance to the values arising from the predicted α_i constants. This disparity constitutes further evidence that the observed levels are either better assigned as $\nu_5+\nu_6$ or in the very least that the resonance mixing is prodigious. By fitting Q-branch frequencies in the ν_5, ν_6, ν_7, and ν_8 fundamental bands of H_2CCO, Duncan and Ferguson[26] also obtained $-\Delta(A_5-B_5)=-1126(10)$,

TABLE XIII. Coriolis and centrifugal distortion constants for H_2CCO and D_2CCO.[a]

H_2CCO ij $\lvert\zeta^a_{ij}\rvert$	ij $\lvert\zeta^b_{ij}\rvert$		ij $\lvert\zeta^c_{ij}\rvert$	
75 (0.671)	51 (0.382)	61 (0.356)	71 (0.054)	83 (0.003)
76 (0.562)	52 (0.614)	62 (0.776)	72 (0.062)	84 (0.243)
85 (0.098)	53 (0.653)	63 (0.521)	73 (0.949)	91 (0.577)
86 (0.715)	54 (0.226)	64 (0.001)	74 (0.305)	92 (0.817)
95 (0.735)			81 (0.792)	93 (0.022)
96 (0.417)			82 (0.560)	94 (0.003)
D_J=0.003 253	D_{JK}=0.485 3		D_K=21.071	
d_1=−0.000 130	d_2=−0.000 047			
H_J=-4.6×10^{-10}	H_{JK}=2.9×10^{-6}		H_{KJ}=−0.000 75	H_K=0.006 14
h_1=2.6×10^{-11}	h_2=4.0×10^{-10}		h_3=7.9×10^{-11}	
D_2CCO ij $\lvert\zeta^a_{ij}\rvert$	ij $\lvert\zeta^b_{ij}\rvert$		ij $\lvert\zeta^c_{ij}\rvert$	
75 (0.074)	51 (0.297)	61 (0.593)	71 (0.179)	83 (0.067)
76 (0.887)	52 (0.932)	62 (0.055)	72 (0.045)	84 (0.281)
85 (0.713)	53 (0.019)	63 (0.585)	73 (0.622)	91 (0.428)
86 (0.367)	54 (0.207)	64 (0.551)	74 (0.761)	92 (0.900)
95 (0.698)			81 (0.855)	93 (0.030)
96 (0.281)			82 (0.431)	94 (0.072)
D_J=0.002 451	D_{JK}=0.323 5		D_K=5.073	
d_1=−0.000 199	d_2=−0.000 100			
H_J=-1.2×10^{-9}	H_{JK}=2.1×10^{-6}		H_{KJ}=−0.000 15	H_K=0.000 82
h_1=-2.1×10^{-11}	h_2=9.2×10^{-10}		h_3=2.2×10^{-10}	

[a]Computed from the QZ(2d,2p) SQM(CCSD)+MP2//EXPT anharmonic force field; centrifugal distortion constants in MHz.

$-\Delta(A_6-\bar{B}_6)=28(40)$, $-\Delta(A_7-\bar{B}_7)=63(49)$, and $-\Delta(A_8-B_8)=-548(11)$, in 10^{-3} cm^{-1} units. The corresponding quantities from Table XII, $\delta_i^\alpha=\alpha_i^A-\frac{1}{2}(\alpha_i^B+\alpha_i^C)$, are $\delta_5^\alpha=-1218$, $\delta_6^\alpha=-442$, $\delta_7^\alpha=117$, and $\delta_8^\alpha=-515$. Even though the empirical $-\Delta(A-B)$ shifts for modes 5 and 8 are immense, the δ_i^α predictions account for them remarkably well. The ill-determined counterparts for modes 6 and 7 are not similarly validated, however.

For D_2CCO the data for vibration–rotation interaction parameters are quite limited. The 1987 high-resolution infrared study of Hegelund *et al.*[30] yielded (B,C) rotational-constant shifts for the ν_5, ν_6, and ν_9 fundamentals as follows (in 10^{-3} cm^{-1} units): $-(\Delta B_5,\Delta C_5)=(-0.140,\ -0.569)$, $-(\Delta B_6,\Delta C_6)=(0.116,\ -0.743)$, and $-(\Delta B_9,\Delta C_9)=(-1.415,\ -0.363)$, in excellent agreement with the predicted constants $(\alpha_5^B,\alpha_5^C)=(-0.169,-0.568)$, $(\alpha_6^B,\alpha_6^C)=(0.023,-0.778)$, and $(\alpha_9^B,\alpha_9^C)=(-1.408,\ -0.377)$. Excited-state A constants were also extracted in the empirical analysis by means of a first-order Coriolis tetrad treatment, but even after deperturbing the $\alpha^A_{5,6,9}$ predictions in Table XII, consistency between theory and experiment is not achieved. Likewise, the $-\Delta(A_2-B_2)$ and $-\Delta(A_4-B_4)$ experimental values of Duncan *et al.*,[27] which involve upper states strongly perturbed by Fermi resonances, are at variance with the predicted δ_2^α and δ_4^α quantities.

IX. CORIOLIS AND CENTRIFUGAL DISTORTION PARAMETERS

The determination of Coriolis constants by direct spectroscopic analysis has been essentially limited to the work of Nemes,[23] who ascertained four a-axis parameters for H_2CCO, viz., $\zeta^a_{58}=+0.33(5)$, $\zeta^a_{68}=+0.714(20)$, $\zeta^a_{59}=-0.774(20)$, and $\zeta^a_{69}=-0.30(2)$. In the empirical GHFF investigation of Duncan and co-workers,[28] the large ζ^a_{68} and ζ^a_{59} constants were found to be useful for refinement of the quadratic force field, whereas the smaller ζ^a_{58} and ζ^a_{69} quantities were surmised to be poorly determined by the available spectroscopic data. Recent high-resolution studies[24,30] of the rovibrational spectrum of ketene-d_2 have utilized Coriolis constants computed directly from empirical force fields.[22,28]

A complete set of revised Coriolis parameters for H_2CCO and D_2CCO, as given by the QZ(2d,2p) SQM(CCSD)+MP2//EXPT force field, is listed in Table XIII. The differences relative to the computed empirical GHFF values[28] are less than 10% in most cases, the average absolute deviation being 0.013 for the parent and 0.034 for the deuterated isotopomer. The most significant variances in the individual parameter sets are exhibited by ζ^c_{83} (0.003 vs 0.031) and ζ^a_{86} (0.367 vs 0.260) for H_2CCO and D_2CCO, respectively. The assessment of Duncan *et al.*[28] regarding the four Coriolis constants of Nemes[23] is corroborated by the current data, and, in fact, the direct spectroscopic value of ζ^a_{59} is even more consistent with the present quadratic force field.

Successive empirical determinations[20,21,25,31,33] of the centrifugal distortion constants of the ground vibrational state of ketene have appeared as the experimental data base of rotational levels has burgeoned. The most recent work,[33] reported in 1992, included 250 millimeter-wave rotational data, 1700 Fourier transform combination differences, and 300 difference-frequency combination differences for (J,K_a) up to (50,9) and entailed a fit to Watson A- and S-reduced (I^r) Hamiltonians containing 5 quartic, 4 sextic, and 2 octic distortion constants. A chronological accounting of the S-reduced (D_K,d_2,H_{KJ},H_{JK}) values and their A-reduced counterparts reveals the sensitivity of these constants to the details of the fit. In fact, the (D_K,d_2) pair has been constrained by normal coordinate calculations in the refinement of distortion constants for some isotopomers.[21,31] In the latest analysis of H_2CCO,[33] the H_J and H_K constants are rather poorly determined, and the (A,D_K,H_K) set is strongly correlated.

The effects of various truncations of the rotational Hamiltonian on the quartic distortion parameters were investigated in some detail by Duncan *et al.*[28] after serious problems were encountered in deriving a physically realistic force field to fit the literature values of these constants simultaneously with the harmonic frequency set of isotopic ketenes. The unresolvable discrepancies of the observed A-reduced quartic constants with respect to the predictions of the final empirical GHFF were approximately 1%(Δ_J), 3%(Δ_{JK}), 12%–15%(Δ_K), 8%(δ_J), and 8%(δ_K). These errors were attributed primarily to the anharmonicity of zero-point vibrational motion, which leads to 10–35 MHz misfits of the planarity condition satisfied by equilibrium quartic distortion constants. Zero-point effects of such an extent have indeed been documented in systematic *ab initio* studies of vibrational anharmonicity.[99,110]

The QZ(2d,2p) SQM(CCSD)+MP2//EXPT force field facilitates not only the reevaluation of quartic centrifugal dis-

tortion constants but also the first direct computation of all sextic parameters, whose determination requires the cubic terms of the potential energy surface. In Table XIII the predicted distortion constants for H_2CCO and D_2CCO are reported for the *S*-reduced Hamiltonian, which exhibits a slight advantage over the *A*-reduced form in empirical refinements.[33] The defining equation for the set of parameters is

$$\begin{aligned}\hat{H}_{\rm rot}^{(S)} = &\left[A-\left(\frac{B+C}{2}\right)\right]\hat{J}_z^2+\left(\frac{B+C}{2}\right)\hat{J}^2-D_J\hat{J}^4-D_{JK}\hat{J}^2\hat{J}_z^2\\ &-D_K\hat{J}_z^4+H_J\hat{J}^6+H_{JK}\hat{J}^4\hat{J}_z^2+H_{KJ}\hat{J}^2\hat{J}_z^4+H_K\hat{J}_z^6\\ &+\left[\left(\frac{B-C}{4}\right)+d_1\hat{J}^2+h_1\hat{J}^4\right](\hat{J}_+^2+\hat{J}_-^2)\\ &+(d_2+h_2\hat{J}^2)(\hat{J}_+^4+\hat{J}_-^4)+h_3(\hat{J}_+^6+\hat{J}_-^6). \qquad (17)\end{aligned}$$

Formulas for the individual distortion constants, which are rather involved for sextic terms, are reported elsewhere,[97,140] and the implementation of these equations with *ab initio* anharmonic force fields has been tested extensively for molecular paradigms.[99] The complementary quartic distortion constants for the *A*-reduced representation are obtained readily from the relations[97] $\Delta_J=D_J-2d_2$, $\Delta_{JK}=D_{JK}+12d_2$, $\Delta_K=D_K-10d_2$, $\delta_K=-4\sigma d_2$, and $\delta_J=-d_1$, where the asymmetry parameter σ is equivalent here to (1441.36, 467.15) for (H_2CCO, D_2CCO).

The 1992 experimental analysis of Johns and co-workers[33] provided the following centrifugal distortion constants (in MHz) for H_2CCO: $D_J=0.003\,278\,96(122)$ [0.8%], $D_{JK}=0.479\,180(97)$ [1.3%], $D_K=22.840(55)$ [7.8%], $d_1=-0.000\,147\,46(23)$ [12%], $d_2=-0.000\,056\,328(55)$ [17%], $H_J\times10^6=-0.002\,04(52)$ [77%], $H_{JK}\times10^6=2.059(65)$ [41%], $H_{KJ}\times10^6=-467.5(30)$ [60%], and $H_K=0.005\,23(159)$ [17%], where standard errors of the fit are given in parentheses and percent errors of the corresponding theoretical values in Table XIII are listed in brackets. The level of agreement with theory for the quartic parameters is comparable to that mentioned above for the empirical GHFF; significant improvements will require consideration of zero-point vibrational effects. The percent errors for the sextic terms are in accord with the magnitudes of variation observed in various empirical fits of these constants. The complete set of sextic parameters derived from the QZ($2d,2p$) SQM(CCSD)+MP2//EXPT force field should aid future empirical analyses by providing an indication of physically realistic solutions. In this regard it is gratifying that the force field predicts minuscule values for the experimentally undetermined h_1, h_2, and h_3 constants.

The centrifugal distortion constants of ground-state D_2CCO were most recently determined by Brown *et al.*,[31] who refitted the microwave data of Nemes and Winnewisser[21] to an *S*-reduced Hamiltonian. Except for d_2, the resulting parameters agree with the quantities in Table XIII substantially better than in the H_2CCO case; e.g., both of the H_{JK} and H_{KJ} discrepancies are only about 30%. Presumably the source of this improvement is a diminution of the anharmonicity of zero-point vibrations upon isotopic substitution. A caveat must be noted, however. The D_K quantity of D_2CCO was constrained in the experimental analysis[31] to a value quoted as 22.540 MHz, an apparent error. By comparison, Duncan and co-workers[28] ascertained $\Delta_K=5.391$ MHz in an independent fit of available microwave and infrared data, which essentially equates to a D_K constant of the same value because d_2 is insignificant. The QZ($2d,2p$) SQM(CCSD)+MP2//EXPT force field yields $D_K(D_2CCO)=5.073$ MHz, vitiating any value which is larger by significantly more than 10%.

X. R_e STRUCTURE

Some of the earliest work on the geometric structure of ketene was a 1938 gas-phase electron diffraction study[141] which determined the heavy-atom distances r(C═C)=1.35 ±0.02 Å and r(C═O)=1.17±0.02 Å. Microwave rotational constants for H_2CCO, HDCCO, and D_2CCO were measured in 1950, from which a favored set of parameters, r(C═C) =1.333 Å, r(C═O)=1.15 Å, and θ(H–C–H)=122.5° was surmised.[6] Despite an ensuing, tentative microwave report giving unphysical structural estimates,[7] improvements in the geometric parameters of ketene were achieved roughly a decade later with the aid of rotational constants from infrared band analyses and new microwave data for the $H_2{}^{13}CCO$ and $H_2CC{}^{18}O$ isotopomers.[13,14,17] Most notable was the Kraitchman analysis of Cox *et al.*[14] in 1959 based on B_0 and C_0 values for four isotopomers, resulting in r(C═C)=1.314 Å, r(C═O)=1.161 Å, r(C–H)=1.083 Å, and θ(H–C–H) =122.6°. Some 17 years later, Mallinson and Nemes[22] derived an empirical quadratic force field for ketene and employed it in more detailed structural analyses. For H_2CCO, HDCCO, and D_2CCO, rotational constants were taken from the 1972 work of Johns *et al.*,[20] as well as unpublished data, whereas for $H_2{}^{13}CCO$ and $H_2CC{}^{18}O$, the aforementioned results from 1959 were utilized. In performing r_0 and r_z structural refinements, allowance was made for the effective mass dependence of selected geometric variables by means of relevant constraints such as r_0(C–D)=r_0(C–H)−0.0015 Å. The r_0, r_s, and r_z parameters deduced for H_2CCO appear in Table I as set (*c*, 1976).

Although the decade after 1976 produced no significant progress in improving the set of rotational constants for isotopic ketenes, renewed structural work was made possible in 1986 and 1987 by the high-resolution infrared studies of Hegelund and co-workers[24,30] on the low-lying *B*- and *C*-type fundamentals of D_2CCO. By supplementing the available microwave data with over 2800 infrared energy level differences, an extremely precise set of D_2CCO rotational constants was determined. Concurrently, the empirical GHFF analysis discussed in Sec. IV provided the first physically acceptable quadratic force field for ketene, prompting Duncan and Munro[29] to revisit the geometric structure in 1987. These authors emphasized that microwave data alone give relatively poor estimates of A_0 because only $\Delta K_a=0$ transitions are strong in near prolate asymmetric rotors such as ketene, making $\Delta K_a=2$ differences from *B*-type infrared fundamental bands critical to the determination of *a*-axis constants. After selecting a preferred data set of rotational constants, corrections due to vibrational, centrifugal distortion, and electronic effects were utilized to obtain zero-point

inertial moments, $I_z^{A,B,C}$, for five isotopic ketenes. From the mean square vibrational amplitudes predicted by the empirical GHFF, isotopic changes (δr_z) in the effective bond lengths were computed. By constraining δr_z(C–H), δr_z(C═C), and δr_z(C═O) shifts to their computed values, assuming no isotopic change in θ_z(H–C–H), but allowing independent variation of δr_z(C–D), an extremely good fit of the $I_z^{A,B,C}$ moments was achieved with the r_z geometric parameters labeled (*b*, 1987) in Table I. Finally, a diatomic model for bond anharmonicity and approximate Morse anharmonicity parameters were employed to estimate the equilibrium coordinates r_e(C–H)=1.0753(17) Å, r_e(C═C) =1.3142(5) Å, r_e(C═O)=1.1609(4) Å, and θ_e(H–C–H)=121.76(33)°.

As of 1990, a dearth of information on $H_2C^{13}CO$ remained, and for $H_2{}^{13}CCO$ and $H_2CC^{18}O$, the B_0 and C_0 constants of Cox *et al.*[14] were still the best available, despite their limited accuracy. The determination of a precise set of rotational constants for these species is paramount to achieving an ultimate solution for the geometric structure of ketene, and this task was finally accomplished in the 1990 microwave investigation of Brown and co-workers.[31] After refitting earlier microwave and infrared combination differences for the parent and deuterated species to an *S*-reduced Hamiltonian and similarly refining parameters on the new data for the heavy-atom variants, a complete set of $A_0^{(S)}$, $B_0^{(S)}$, and $C_0^{(S)}$ constants for H_2CCO, $H_2C^{13}CO$, $H_2{}^{13}CCO$, $H_2CC^{18}O$, HDCCO, and D_2CCO was ascertained. The resulting r_0 and r_s structures are specified in Table I as (*a*, 1990) entries. In addition, the approximation $I_e \approx 2I_s - I_0$ was invoked to obtain the r_e estimates denoted as r_m^ρ in the table.

The present derivation of the QZ(2*d*,2*p*) SQM(CCSD) +MP2//EXPT anharmonic force field allows a high-precision r_e structure of ketene to be extracted by first principles for the first time. In Table XIV the information required for this procedure is collected. The very recent, comprehensive analysis of Johns and collaborators,[33] discussed in Sec. IX, of the myriad microwave and infrared data of H_2CCO is the source of the $A_0^{(S)}$, $B_0^{(S)}$, and $C_0^{(S)}$ values for the parent molecule. The 1990 work of Brown *et al.*[31] provides the rotational constants for the five complementary isotopomers.

The small centrifugal distortion corrections to the empirical rotational constants were evaluated theoretically from the quadratic force field according to

$$A_0 = A_0^{(S)} - 6R_6 + 5\sigma^{-1}R_5 - 4^{-1}(3\tau_{bcbc} - 2\tau_{caca} - 2\tau_{abab}), \tag{18}$$

$$B_0 = B_0^{(S)} + 4R_6 - 2(2+\sigma^{-1})R_5 - 4^{-1}(3\tau_{caca} - 2\tau_{abab} - 2\tau_{bcbc}), \tag{19}$$

and

$$C_0 = C_0^{(S)} + 4R_6 + 2(2-\sigma^{-1})R_5 - 4^{-1}(3\tau_{abab} - 2\tau_{bcbc} - 2\tau_{caca}), \tag{20}$$

where R_5, R_6, and $\tau_{\alpha\beta\alpha\beta}$ denote the usual quartic distortion parameters,[97,98] and the inverse asymmetry quantity $\sigma^{-1} = (B_0' - C_0')(2A_0' - B_0' - C_0')^{-1}$ is derived from the effective rotational constants of the Kivelson and Wilson formalism.[99,142] The more substantial zero-point vibrational contributions to the A_0, B_0, and C_0 constants, ranging from 0.2% to 0.6%, were computed as one-half the sums of the associated QZ(2*d*,2*p*) SQM(CCSD)+MP2//EXPT vibration–rotation interaction parameters (α_i) for each isotopomer. Although individual α_i^A constants are adversely affected by the *a*-type Coriolis resonances occurring within the (ν_5, ν_6, ν_8, ν_9) manifold, the $A_e - A_0$ differences are invariant to these perturbations. In particular, the *net* Coriolis contribution to $A_e - A_0$ is of the form[103]

$$A_e^2 \sum_{i>j} \frac{(\zeta_{ij}^a)^2(\omega_i - \omega_j)^2}{\omega_i\omega_j(\omega_i + \omega_j)}, \tag{21}$$

which is devoid of resonance denominators. The coupling of electronic orbital angular momentum with rotation of the nuclear framework engenders an additional term for the moments of inertia which is aggrandized by off-axis lone-pair or π electrons.[96,143] The corresponding $\Delta I_{\rm elec}^{A,B,C}$ corrections are derivable via measurements of the molecular rotational Zeeman effect, and the values assumed here were taken directly from Duncan and Munro.[29]

The I_e moments obtained for H_2CCO display an inertial defect (Δ_e) which is almost 300 times smaller than that for the I_0 values and an order of magnitude smaller than the I_z defect. Larger Δ_e quantities are generally found for the other isotopomers due to much greater uncertainties in the $A_0^{(S)}$ constants, the $H_2CC^{18}O$ species constituting the extreme in this regard. Because the inertial defect for $H_2CC^{18}O$ (0.032 amu Å^2) exceeds that for any other isotopomer by a factor of 17, the $A_0^{(S)}$ value for this species was omitted from the structural analysis.

In order to achieve both a reliable and internally consistent structure determination, four independent methods were employed to extract r_e parameters from the empirically derived I_e moments of inertia. In methods I and II, a least-squares fit of the internal variables was performed to the (I_e^A, I_e^B, I_e^C) and (I_e^B, I_e^C) isotopomeric sets of moments, respectively, excluding $I_e^A(H_2CC^{18}O)$ in the former case. In methods III and IV, the r_e parameters were computed from the nuclear positions (a_i, b_i) in the principal-axis system, as ascertained by applying the Kraitchman[144] equations to the (I_e^B, I_e^C) data set with D_2CCO and HDCCO moments, respectively, used to locate the hydrogen atoms.[145] As in essentially all previous work on the substitution structure of ketene, the consistency of the procedure for methods III and IV was optimized by replacing explicit I_e^A data with $I_e^C - I_e^B$ values and imposing a first-moment condition to pinpoint the central carbon. These modifications overcome numerical deteriorations brought on by the relative uncertainty of the I_e^A moments[31,146] as well as the near coincidence of the central carbon ($a_C = -0.021$ Å) and the molecular center of mass. The assumed linearity of the C═C═O chain was confirmed by the finding of very small real and imaginary Kraitchman *b* coordinates for these atoms whose magnitudes were well below the inherent uncertainties.

The r_e(C═O), r_e(C═C), r_e(C–H), and θ_e(H–C–H) values derived by methods I–IV are given in Table I,

TABLE XIV. Derivation of the equilibrium moments of inertia for the isotopomers of ketene.[a]

	H_2CCO	$H_2C^{13}CO$	$H_2{}^{13}CCO$	$H_2CC^{18}O$	HDCCO	D_2CCO
$A_0^{(S)}$	9.409 883 (14)	9.417 65 (1738)	9.410 24 (1114)	9.584 96 (3035)	6.481 32 (127)	4.721 17 (40)
$B_0^{(S)}$	0.343 348 24(3)	0.343 358 23(19)	0.332 262 06(26)	0.325 599 81(11)	0.321 791 50(4)	0.304 238 13(5)
$C_0^{(S)}$	0.330 759 00(3)	0.330 768 98(19)	0.320 459 28(28)	0.314 254 86(11)	0.306 033 24(4)	0.285 287 39(5)
$A_0 - A_0^{(S)}$	−0.000 017 6	−0.000 017 6	−0.000 016 5	−0.000 016 0	−0.000 014 4	−0.000 012 2
$B_0 - B_0^{(S)}$	−0.000 000 96	−0.000 000 96	−0.000 000 90	−0.000 000 87	−0.000 001 38	−0.000 000 78
$C_0 - C_0^{(S)}$	0.000 042 88	0.000 042 87	0.000 040 21	0.000 039 16	0.000 034 57	0.000 029 61
$A_e - A_0$	0.055 17	0.055 63	0.055 89	0.055 21	0.020 37	0.015 52
$B_e - B_0$	0.000 920 45	0.000 906 29	0.000 892 12	0.000 866 25	0.000 795 52	0.000 670 70
$C_e - C_0$	0.001 389 80	0.001 375 96	0.001 331 89	0.001 292 32	0.001 269 76	0.001 146 91
ΔI_{elec}^A	0.000 408	0.000 408	0.000 408	0.000 408	0.000 600	0.000 840
ΔI_{elec}^B	0.000 952	0.000 952	0.000 952	0.000 952	0.001 020	0.001 090
ΔI_{elec}^C	0.000 661	0.000 661	0.000 661	0.000 661	0.000 750	0.000 809
I_e^A	1.780 634 (3)	1.779 09 (330)	1.780 43 (212)	1.748 28 (557)	2.592 215 (509)	3.558 122 (303)
I_e^B	48.965 678 (4)	48.966 270 (28)	50.599 272 (40)	51.635 886 (18)	52.256 826 (7)	55.286 498 (9)
I_e^C	50.746 035 (4)	50.746 627 (29)	52.379 658 (46)	53.416 197 (19)	54.849 786 (8)	58.846 501 (11)
Δ_e	−0.000 28	0.001 27	−0.000 05	0.032 03	0.000 75	0.001 88

[a]Data for rotational constants in cm^{-1} and moments of inertia in amu $Å^2$. The empirical constants $A_0^{(S)}$, $B_0^{(S)}$, and $C_0^{(S)}$, which refer to an *S*-reduced Hamiltonian in the I^r representation, are selected from Ref. 33 for the parent molecule and from Ref. 31 for its isotopic variants. The vibrational and centrifugal distortion contributions are computed from the QZ(2*d*,2*p*) SQM(CCSD)+MP2//EXPT anharmonic force field. The electronic corrections to the moments of inertia are taken from Ref. 29. The inertial defects in the final I_e^A, I_e^B, and I_e^C values are listed as Δ_e entries.

wherein the observed ranges of variation are only 0.000 07 Å, 0.000 11 Å, 0.000 50 Å, and 0.052°, respectively. In brief, the consistency exhibited by the r_e predictions is remarkable. Because method I incorporates all rotational-constant data except $A_0^{(S)}(H_2CC^{18}O)$ in the structural refinement, the r_e(I; ls-*ABC*) parameters are recommended here as final values. Nevertheless, there are no statistically significant differences between the r_e(I; ls-*ABC*) and r_e(II; ls-*BC*) results, implying that the sizeable zero-point vibrational contributions to the A_0 constants are properly accounted for in the analysis. The diminutive standard errors from the r_e(I; ls-*ABC*) fit suggest that ketene is now exemplary of the best determined equilibrium molecular structures to date.

The r_e structural estimates of Duncan and Munro[29] are in excellent accord with the current r_e(I; ls-*ABC*) parameters, perhaps excepting the instance of r_e(C═C), for which the +0.0021 Å deviation is ~4 times larger than their quoted uncertainty. The alternative $r_m^{(2)}$ approximations to the r_e parameters (Table I) are slightly better for the heavy-atom distances and noticeably poorer for the methylene coordinates, yet within the stated uncertainties in all cases. As expected from simple anharmonicity considerations, all geometric quantities in the empirical r_0, r_s, and r_z structures exceed their r_e counterparts, the differences being most pronounced for the two hydrogen-related variables. Specifically, the vibration-induced shifts of [r(C═O), r(C═C), r(C–H), θ(H–C–H)] relative to the equilibrium values are (in Å, deg) r_0(+0.0023, +0.0026, +0.0147, +1.679°), r_s(+0.0017, +0.0016, +0.0067, +0.779°), and r_z(+0.0011, +0.0044, +0.0043, +0.197°), where structures (*a*, 1990) and (*b*, 1987) from Table I are assumed for the comparison. The large deviations in the r_0(C–H) and θ_0(H–C–H) values of the (*a*, 1990) and (*c*, 1976) studies result primarily from the use of mass dependent parameters in the (*c*, 1976) refinement.

Considering the level of accuracy normally achieved by *ab initio* structural predictions in multiply bonded systems, the DZP CISD, QZ(2*d*,2*p*) CCSD, and QZ(2*d*1*f*,2*p*1*d*) CCSD(T) equilibrium data in Table I compare very favorably with the high-precision r_e(I; ls-*ABC*) parameters. For the bond lengths, the QZ(2*d*,2*p*) CCSD method happens to exhibit a superior cancellation of basis set and electron correlation errors,[147] the disparities in r_e(C═O), r_e(C═C), and r_e(C–H) being only −0.0006, 0.0034, and <0.0001 Å, respectively. The degree to which the DZP CISD results fortuitously mimic the higher-quality QZ(2*d*1*f*,2*p*1*d*) CCSD(T) predictions is equally remarkable. The +0.0055 and +0.0068 Å overestimations of r_e(C═O) and r_e(C═C) at the QZ(2*d*1*f*,2*p*1*d*) CCSD(T) level of theory are very similar to the +0.0063 Å error found for the cc-pVTZ CCSD(T) bond length of carbon dioxide.[115] Upon extending the one-particle basis to *spdfg* quality by means of cc-pVQZ CCSD(T) computations, the bond length error in CO_2 is reduced to only +0.0026 Å,[115] the bulk of which is attributable to core correlation effects.[148,149] Indeed, for the multiply bonded first-row diatomics N_2, O_2, CO, and NO, the magnitudes of the established r_e contractions due to 1*s* correlation

are 0.0019–0.0023 Å.[149] Proportionate reductions due to basis set and core correlation effects are anticipated for the QZ($2d1f,2p1d$) CCSD(T) error in r_e(C–H) of ketene (+0.0024 Å), as evidenced by another high-level theoretical study of formaldehyde,[116] *inter alia*. In summary, clear precedents exist to rationalize the systematic approach of *ab initio* predictions from the QZ($2d1f,2p1d$) CCSD(T) equilibrium geometry to the final r_e(I; ls-ABC) structure.

Finally, a few chemically significant observations regarding the equilibrium structure of ketene are apt. The proximity of the r_e(C═O) distances in ketene and carbon dioxide[138,150] is striking (0.0003 Å), these parameters being coincident within experimental uncertainty. The r_e(C═C) distance for ketene is 0.024 Å shorter than that for ethylene,[99] and a comparison of r_z parameters suggests that it exceeds the analogous length in allene by about 0.007 Å.[136] A similar perusal of carbon–hydrogen distances[99,136] reveals that ketene and ethylene have r_e(C–H) values differing by less than 0.001 Å, whereas the bond length in allene is ~0.006 Å longer. Certainly the most intriguing aspect of the ketene structure is the occurrence of a valence bond angle for the methylene framework which is greater than 120° by a chemically substantial amount. This unusual phenomenon is not found in the related species formaldehyde,[151] ethylene,[99] allene,[136] or C_{2v}-constrained propadienone,[152,153] although diazomethane exhibits the effect to an even greater extent.[154]

The significance of the large H–C–H angle in ketene appears to have escaped notice in previous spectroscopic investigations, particularly with respect to the θ_e(H–C–H) trend found in the isoelectronic series ($H_2C{=}C{=}CH_2 \rightarrow H_2C{=}C{=}O \rightarrow H_2C{=}N{=}N$). The chemical origins of this trend are exposed if a natural bond orbital (NBO) analysis[155] is performed on the RHF one-particle density matrix computed with the 6-31G** basis set.[156] Drastic differences in electronic structure are revealed by the representations of the two in-plane, π-type canonical molecular orbitals (ϕ_i) in the basis of (σ,π) natural bond orbitals:

allene[θ_e(H–C–H)=118.27°]:

$$\phi_8(b_2)=0.292\pi(C_2{=}C_1)+0.946(2^{-1/2})[\sigma(C_3{-}H_4)-\sigma(C_3{-}H_5)], \tag{22}$$

$$\phi_{10}(b_2)=0.951\pi(C_2{=}C_1)-0.291(2^{-1/2})[\sigma(C_3{-}H_4)-\sigma(C_3{-}H_5)];$$

ketene[θ_e(H–C–H)=121.78°]:

$$\phi_8(b_2)=0.655\pi(C_2{=}O_1)+0.742(2^{-1/2})[\sigma(C_3{-}H_4)-\sigma(C_3{-}H_5)], \tag{23}$$

$$\phi_{10}(b_2)=0.753\pi(C_2{=}O_1)-0.648(2^{-1/2})[\sigma(C_3{-}H_4)-\sigma(C_3{-}H_5)];$$

diazomethane[θ_e(H–C–H)=126.20°]:

$$\phi_7(b_2)=0.706\pi(N_2{=}N_1)+0.697(2^{-1/2})[\sigma(C_3{-}H_4)-\sigma(C_3{-}H_5)], \tag{24}$$

$$\phi_{10}(b_2)=0.703\pi(N_2{=}N_1)-0.703(2^{-1/2})[\sigma(C_3{-}H_4)-\sigma(C_3{-}H_5)].$$

The numbering scheme of Fig. 2 is assumed in these equations, and the geometric structures of allene[136] and diazomethane[157] used in the 6-31G** RHF computations were taken from experiment. The unmistakable feature of the NBO reconstructions is the extensive delocalization of b_2 molecular orbitals which attends large θ_e values over 120°, a consequence of strong hyperconjugative interactions of the σ(C–H) bonds with the in-plane π network. To elucidate this behavior further, the 6-31G** RHF data were extended to include results for each molecule at each equilibrium angle within the series. The various E_{RHF} values were then decomposed according to the exact relation[67]

$$E_{\mathrm{RHF}}=\sum_i^{\mathrm{occ}}(h_{ii}+\epsilon_i+\bar{\nu}_{\mathrm{rep}})=2\sum_i^{\mathrm{occ}}\lambda_i, \tag{25}$$

where i runs over the 11 doubly occupied spatial orbitals, the ϵ_i quantities are orbital energies, h_{ii} denotes diagonal matrix elements of the one-electron Hamiltonian in the molecular orbital basis, $\bar{\nu}_{\mathrm{rep}}$ is the nuclear repulsion energy partitioned per electron pair, and $\lambda_i=(1/2)(h_{ii}+\epsilon_i+\bar{\nu}_{\mathrm{rep}})$ is the total energy attributable to an α or β electron in orbital i. The $2\Delta\lambda_i$ shifts resulting from increases of θ(H–C–H) with fixed bond distances can be summed over symmetry species to yield conformational energy changes ΔE_λ arising individually from the (a_1,b_1,b_2) orbital spaces. In this manner, the total ΔE_{RHF} differences for θ variations for a reference structure were precisely partitioned into the consequences of $\sigma(a_1)$, $\pi_{op}(b_1)$, and $\pi_{ip}(b_2)$ orbital reorganizations:

allene θ[118.27°→121.78°]:

$$2(\Delta\lambda_8,\Delta\lambda_{10})=(-7.0,-1.8)\ \text{kcal mol}^{-1}, \tag{26}$$

$$[\Delta E_\lambda(a_1,b_1,b_2);\Delta E_{\mathrm{RHF}}]=[(+18.13,-8.86,-8.86);+0.432]\ \text{kcal mol}^{-1};$$

ketene θ[118.27°→121.78°]:

$$2(\Delta\lambda_8,\Delta\lambda_{10})=(+46.0,-58.0)\ \text{kcal mol}^{-1}, \tag{27}$$

$$[\Delta E_\lambda(a_1,b_1,b_2);\Delta E_{\mathrm{RHF}}]=[(+8.53,+3.30,-12.00);-0.196]\ \text{kcal mol}^{-1};$$

diazomethane θ[118.27°→126.20°]:

$$2(\Delta\lambda_7,\Delta\lambda_{10})=(+59.2,-87.9)\ \text{kcal mol}^{-1}, \tag{28}$$

$$[\Delta E_\lambda(a_1,b_1,b_2);\Delta E_{\mathrm{RHF}}]=[(+17.93,+9.93,-28.68);-0.765]\ \text{kcal mol}^{-1}.$$

As quantified in Eqs. (27) and (28), the delocalized orbital $\phi_{10}(b_2)$ of ketene and diazomethane provides an immense driving force ($2\Delta\lambda_{10}$) for θ increase which is paramount to

overcoming not only net $\sigma(a_1)$ and $\pi_{op}(b_1)$ destabilizations but also a sizeable compensating term $(2\Delta\lambda_{8,7})$ due to $\phi_{8,7}(b_2)$. Accordingly, the total energy of these molecules is lowered as θ is increased from the equilibrium angle of allene. No similar driving force exists in allene, where the mixing of $\pi(C_2{=}C_1)$ and $(2^{-1/2})[\sigma(C_3{-}H_4){-}\sigma(C_3{-}H_5)]$ is quite limited. Apparently, a near perfect resonance of the occupied, in-plane π component of the cumulated network with the antisymmetric σ(C–H) bonding orbital is necessary to generate a considerable propensity for widened methylene angles, at least in the absence of inductive effects arising from pronounced electronegativity differences.[158] However, this inference does not require that delocalization within the in-plane π space is necessarily enhanced as θ increases. In ketene, the mixture of π(C═O) and σ(C–H) in $\phi_{10}(b_2)$ is (53.4%, 45.1%) at $\theta_e=118.27°$ but is diminished to (56.7%, 42.0%) at $\theta_e=121.78°$; nonetheless, in diazomethane this mixing is increased from (44.8%, 53.9%) to (49.4%, 49.4%) as θ_e goes from 118.27° to 126.20°. Clearly the geometric structures within the isoelectronic series ($H_2C{=}C{=}CH_2 \rightarrow H_2C{=}C{=}O \rightarrow H_2C{=}N{=}N$) are manifestations of intricate electronic structure effects.

XI. SUMMARY

The traditional but elusive spectroscopic goal of ascertaining a complete anharmonic force field which faithfully reproduces the detailed structure of the rovibrational eigenstates of the penta-atomic ketene molecule has been pursued in this investigation by means of high-level *ab initio* computations subjected to a limited empirical scaling of quadratic parameters on the fundamental frequencies of isotopic ketenes. Accurate harmonic vibrational frequencies and quadratic force constants of ketene are thus established and subsequently scrutinized for chemically significant features. The physical origins of the associated anharmonicities are exposed, and the higher-order force constants of consequence in the quartic force field are rigorously distinguished from those which have essentially no bearing on the vibrational dynamics. Model diad and tetrad Hamiltonians are employed to treat prominent vibrational resonances in first order and deperturb the corresponding spectral bands. The assignment of selected overtone and combination bands is examined, with particular focus on the implications for abnormal anharmonicity of modes involving substantial bending of the C═C═O framework. The issue of vibration–rotation interaction is explored; the relevant spectroscopic parameters α_i are computed and decomposed into inertial-derivative, anharmonicity, and Coriolis components, the latter being immense for the interaction of C═C═O bending vibrations and a-axis rotations. The determination of not only Coriolis but also quartic and sextic centrifugal distortion constants from the final anharmonic force field provides standards for the assessment of physically realistic results from spectroscopic fits. High-resolution empirical rotational constants for six isotopic ketenes are corrected for the effects of centrifugal distortion, electronic orbital angular momentum, and anharmonic zero-point vibrations and subsequently used to extract the r_e structure of ketene; the small standard errors of the r_e parameters suggest that ketene is now exemplary of the best determined molecular structures to date. Finally, the electronic origin of the peculiar, widened methylene moiety in ketene is revealed by a natural bond orbital analysis.

The anharmonic force field of ketene derived in this investigation provides the groundwork for first-principles theoretical determinations of the rate constant for the dissociation of ketene as a function of total energy and angular momentum, insofar as more accurate computations of densities of high-lying vibrational states are facilitated in the application of statistical reaction-rate theories to this exhaustively studied chemical species. In companion papers,[159,160] the rigorous implementation of a variational RRKM formalism is described which brings theory into quantitative agreement with recent state-to-state experiments. Such studies are providing tests of unprecedented detail in the continuing development and refinement of unimolecular dissociation theories.

[1] H. Kopper, Z. Phys. Chem. B **34**, 396 (1936).
[2] H. Gershinowitz and E. B. Wilson, Jr., J. Chem. Phys. **5**, 500 (1937).
[3] F. Halverson and V. Z. Williams, J. Chem. Phys. **15**, 552 (1947).
[4] W. R. Harp, Jr. and R. S. Rasmussen, J. Chem. Phys. **15**, 778 (1947).
[5] L. G. Drayton and H. W. Thompson, J. Chem. Soc. **1948**, 1416.
[6] B. Bak, E. S. Knudsen, E. Madsen, and J. Rastrup-Andersen, Phys. Rev. **79**, 190 (1950).
[7] H. R. Johnson, J. G. Ingersoll, and M. W. P. Strandberg, Phys. Rev. **82**, 327 (1951).
[8] W. H. Fletcher and W. F. Arendale, J. Chem. Phys. **19**, 1431 (1951).
[9] H. R. Johnson and M. W. P. Strandberg, J. Chem. Phys. **20**, 687 (1952).
[10] B. Bak and F. A. Andersen, J. Chem. Phys. **22**, 1050 (1954).
[11] W. F. Arendale and W. H. Fletcher, J. Chem. Phys. **24**, 581 (1956).
[12] W. F. Arendale and W. H. Fletcher, J. Chem. Phys. **26**, 793 (1957).
[13] P. E. B. Butler, D. R. Eaton, and H. W. Thompson, Spectrochim. Acta **13**, 223 (1958).
[14] A. P. Cox, L. F. Thomas, and J. Sheridan, Spectrochim. Acta **15**, 542 (1959).
[15] S. Sundaram and F. F. Cleveland, J. Chem. Phys. **32**, 1554 (1960).
[16] A. P. Cox and A. S. Esbitt, J. Chem. Phys. **38**, 1636 (1963).
[17] C. B. Moore and G. C. Pimentel, J. Chem. Phys. **38**, 2816 (1963).
[18] W. H. Fletcher and W. T. Thompson, J. Mol. Spectrosc. **25**, 240 (1968).
[19] D. C. McKean and J. L. Duncan, Spectrochim. Acta Part A **27**, 1879 (1971).
[20] J. W. C. Johns, J. M. R. Stone, and G. Winnewisser, J. Mol. Spectrosc. **42**, 523 (1972).
[21] L. Nemes and M. Winnewisser, Z. Naturforsch. Teil A **31**, 272 (1976).
[22] P. D. Mallinson and L. Nemes, J. Mol. Spectrosc. **59**, 470 (1976).
[23] L. Nemes, J. Mol. Spectrosc. **72**, 102 (1978).
[24] F. Winther, F. Hegelund, and L. Nemes, J. Mol. Spectrosc. **117**, 388 (1986).
[25] L. Nemes, J. Demaison, and G. Wlodarczak, Acta Phys. Hungary **61**, 135 (1987).
[26] J. L. Duncan and A. M. Ferguson, Spectrochim. Acta Part A **43**, 1081 (1987).
[27] J. L. Duncan, A. M. Ferguson, J. Harper, K. H. Tonge, and F. Hegelund, J. Mol. Spectrosc. **122**, 72 (1987).
[28] J. L. Duncan, A. M. Ferguson, J. Harper, and K. H. Tonge, J. Mol. Spectrosc. **125**, 196 (1987).
[29] J. L. Duncan and B. Munro, J. Mol. Spectrosc. **161**, 311 (1987).
[30] F. Hegelund, J. Kauppinen, and F. Winther, Mol. Phys. **61**, 261 (1987).
[31] R. D. Brown, P. D. Godfrey, D. McNaughton, A. P. Pierlot, and W. H. Taylor, J. Mol. Spectrosc. **140**, 340 (1990).
[32] R. Escribano, J. Ortigoso, E. Cutín, and I. García-Moreno, J. Chem. Phys. **93**, 9208 (1990).
[33] J. W. C. Johns, L. Nemes, K. M. T. Yamada, T. Y. Wang, J. L. Doménech, J. Santos, P. Cancio, D. Bermejo, J. Ortigoso, and R. Escribano, J. Mol. Spectrosc. **156**, 501 (1992).
[34] D. J. Nesbitt, H. Petek, M. F. Foltz, S. V. Filseth, D. J. Bamford, and C. B. Moore, J. Chem. Phys. **83**, 223 (1985).
[35] H. Bitto, I.-C. Chen, and C. B. Moore, J. Chem. Phys. **85**, 5101 (1986).
[36] H. Bitto, D. R. Guyer, W. F. Polik, and C. B. Moore, Faraday Discuss. Chem. Soc. **82**, 149 (1986).

[37] I.-C. Chen, W. H. Green, Jr., and C. B. Moore, J. Chem. Phys. **89**, 314 (1988).
[38] W. H. Green, Jr., I.-C. Chen, and C. B. Moore, Ber. Bunsenges. Phys. Chem. **92**, 389 (1988).
[39] E. D. Potter, M. Gruebele, L. R. Khundkar, and A. H. Zewail, Chem. Phys. Lett. **164**, 463 (1989).
[40] I.-C. Chen and C. B. Moore, J. Phys. Chem. **94**, 263 (1990).
[41] I.-C. Chen and C. B. Moore, J. Phys. Chem. **94**, 269 (1990).
[42] S. K. Kim, Y. S. Choi, C. D. Pibel, Q.-K. Zheng, and C. B. Moore, J. Chem. Phys. **94**, 1954 (1991).
[43] W. H. Green, Jr., A. J. Mahoney, Q.-K. Zheng, and C. B. Moore, J. Chem. Phys. **94**, 1961 (1991).
[44] W. H. Green, Jr., C. B. Moore, and W. F. Polik, Annu. Rev. Phys. Chem. **43**, 591 (1992).
[45] E. R. Lovejoy, S. K. Kim, and C. B. Moore, Science **256**, 1541 (1992).
[46] R. A. Marcus, Science **256**, 1523 (1992).
[47] I. W. M. Smith, Nature **358**, 279 (1992).
[48] D. M. Wardlaw and R. A. Marcus, Chem. Phys. Lett. **110**, 230 (1984); J. Chem. Phys. **83**, 3462 (1985); Adv. Chem. Phys. **70**, 231 (1988).
[49] R. A. Marcus, Chem. Phys. Lett. **144**, 208 (1988).
[50] S. J. Klippenstein and R. A. Marcus, J. Chem. Phys. **91**, 2280 (1989).
[51] S. J. Klippenstein and R. A. Marcus, J. Chem. Phys. **93**, 2418 (1990).
[52] S. J. Klippenstein and R. A. Marcus, J. Phys. Chem. **92**, 3105 (1988).
[53] S. J. Klippenstein and R. A. Marcus, J. Phys. Chem. **92**, 5412 (1988).
[54] J. Yu and S. J. Klippenstein, J. Phys. Chem. **95**, 9882 (1991).
[55] S. J. Klippenstein, J. Chem. Phys. **94**, 6469 (1991); **96**, 367 (1992).
[56] S. C. Smith, J. Chem. Phys. **97**, 2406 (1992).
[57] S. J. Klippenstein, J. Phys. Chem. **98**, 11 459 (1994).
[58] R. J. Bartlett, Annu. Rev. Phys. Chem. **32**, 359 (1981).
[59] G. D. Purvis and R. J. Bartlett, J. Chem. Phys. **76**, 1910 (1982).
[60] J. Paldus, in *New Horizons of Quantum Chemistry*, edited by P.-O. Löwdin and B. Pullmann (Reidel, Dordrecht, 1983), p. 31.
[61] R. J. Bartlett, C. E. Dykstra, and J. Paldus, in *Advanced Theories and Computational Approaches to the Electronic Structure of Molecules*, edited by C. E. Dykstra (Reidel, Dordrecht, 1984), p. 127.
[62] G. E. Scuseria, A. C. Scheiner, T. J. Lee, J. E. Rice, and H. F. Schaefer III, J. Chem. Phys. **86**, 2881 (1987).
[63] A. C. Scheiner, G. E. Scuseria, J. E. Rice, T. J. Lee, and H. F. Schaefer III, J. Chem. Phys. **87**, 5361 (1987).
[64] C. Møller and M. S. Plesset, Phys. Rev. **46**, 618 (1934).
[65] J. A. Pople, J. S. Binkley, and R. Seeger, Int. J. Quantum Chem. Symp. **10**, 1 (1976).
[66] W. J. Hehre, L. Radom, P. v. R. Schleyer, and J. A. Pople, *Ab Initio Molecular Orbital Theory* (Wiley–Interscience, New York, 1986).
[67] A. Szabo and N. S. Ostlund, *Modern Quantum Chemistry* (McGraw–Hill, New York, 1989).
[68] K. Raghavachari, G. W. Trucks, J. A. Pople, and M. Head-Gordon, Chem. Phys. Lett. **157**, 479 (1989).
[69] G. E. Scuseria and T. J. Lee, J. Chem. Phys. **93**, 5851 (1990).
[70] C. C. J. Roothaan, Rev. Mod. Phys. **23**, 69 (1951).
[71] PSI 2.0, PSITECH, Inc. (1991).
[72] GAUSSIAN92, Revision A, M. J. Frisch, G. W. Trucks, M. Head-Gordon, P. M. W. Gill, M. W. Wong, J. B. Foresman, B. G. Johnson, H. B. Schlegel, M. A. Robb, E. S. Replogle, R. Gomperts, J. L. Andres, K. Raghavachari, J. S. Binkley, C. Gonzalez, R. L. Martin, D. J. Fox, D. J. Defrees, J. Baker, J. J. P. Stewart, and J. A. Pople (Gaussian, Inc., Pittsburgh, PA, 1992).
[73] S. Huzinaga, J. Chem. Phys. **42**, 1293 (1965).
[74] T. H. Dunning, Jr., J. Chem. Phys. **55**, 716 (1971).
[75] W. D. Allen and H. F. Schaefer III, Chem. Phys. **108**, 243 (1986).
[76] T. H. Dunning, Jr., J. Chem. Phys. **90**, 1007 (1989).
[77] A. P. Rendell and T. J. Lee, J. Chem. Phys. **94**, 6219 (1991).
[78] T. J. Lee and A. P. Rendell, J. Chem. Phys. **94**, 6229 (1991).
[79] As usual, // denotes "at the geometry of." The listed MP2 energy involves *d* manifolds comprised of six Cartesian components.
[80] T. J. Lee and P. R. Taylor, Int. J. Quantum Chem. Symp. **23**, 199 (1989).
[81] N. C. Handy, R. D. Amos, J. F. Gaw, J. E. Rice, and E. D. Simandiras, Chem. Phys. Lett. **120**, 151 (1985).
[82] E. D. Simandiras, N. C. Handy, and R. D. Amos, Chem. Phys. Lett. **133**, 324 (1987).
[83] G. Fogarasi and P. Pulay, in *Vibrational Spectra and Structure*, edited by J. R. Durig (Elsevier, Amsterdam, 1985), Vol. 14, p. 125.
[84] P. Pulay, G. Fogarasi, and J. E. Boggs, J. Chem. Phys. **74**, 3999 (1981).
[85] G. Bánhegyi, G. Fogarasi, and P. Pulay, J. Mol. Struct. **89**, 1 (1982).
[86] P. Pulay, G. Fogarasi, G. Pongor, J. E. Boggs, and A. Vargha, J. Am. Chem. Soc. **105**, 7037 (1983).
[87] G. Pongor, P. Pulay, G. Fogarasi, and J. E. Boggs, J. Am. Chem. Soc. **106**, 2765 (1984).
[88] H. Sellers, P. Pulay, and J. E. Boggs, J. Am. Chem. Soc. **107**, 6487 (1985).
[89] W. D. Allen, A. G. Császár, and D. A. Horner, J. Am. Chem. Soc. **114**, 6834 (1992).
[90] P. Pulay and F. Török, Acta Chim. Acad. Sci. Hungary **44**, 287 (1965).
[91] G. Keresztury and G. Jalsovszky, J. Mol. Struct. **10**, 304 (1971).
[92] J. Overend, in *Infrared Spectroscopy and Molecular Structure*, edited by M. Davies (Elsevier, Amsterdam, 1963), p. 345.
[93] G. Zerbi, in *Vibrational Intensities in Infrared and Raman Spectroscopy*, edited by W. B. Person and G. Zerbi (Elsevier, Amsterdam, 1982).
[94] H. H. Nielsen, Rev. Mod. Phys. **23**, 90 (1951).
[95] I. M. Mills, in *Molecular Spectroscopy: Modern Research*, edited by K. N. Rao and C. W. Mathews (Academic, New York, 1972), Vol. 1, p. 115.
[96] D. Papoušek and M. R. Aliev, *Molecular Vibrational–Rotational Spectra* (Elsevier, Amsterdam, 1982).
[97] J. K. G. Watson, in *Vibrational Spectra and Structure*, edited by J. R. Durig (Elsevier, Amsterdam, 1977), Vol. 6, p. 1.
[98] J. K. G. Watson, J. Chem. Phys. **48**, 4517 (1968).
[99] D. A. Clabo, Jr., W. D. Allen, R. B. Remington, Y. Yamaguchi, and H. F. Schaefer III, Chem. Phys. **123**, 187 (1988).
[100] W. D. Allen, Y. Yamaguchi, A. G. Császár, D. A. Clabo, Jr., R. B. Remington, and H. F. Schaefer III, Chem. Phys. **145**, 427 (1990).
[101] W. D. Allen, A. L. L. East, and A. G. Császár, in *Structures and Conformations of Nonrigid Molecules*, edited by J. Laane, M. Dakkouri, B. van der Vecken, and H. Oberhammer (Kluwer, Dordrecht, 1993), p. 343.
[102] W. D. Allen and A. G. Császár, J. Chem. Phys. **98**, 2983 (1993).
[103] A. L. L. East, C. S. Johnson, and W. D. Allen, J. Chem. Phys. **98**, 1299 (1993).
[104] N. E. Klepeis, A. L. L. East, A. G. Császár, W. D. Allen, T. J. Lee, and D. W. Schwenke, J. Chem. Phys. **99**, 3865 (1993).
[105] The investigations cited here (Refs. 106–118) are perforce only representative of work since 1986 and are by no means exhaustive. Many excellent theoretical studies primarily involving variational vibrational procedures on *ab initio* potential energy surfaces are not included.
[106] W. H. Green, D. Jayatilaka, A. Willetts, R. D. Amos, and N. C. Handy, J. Chem. Phys. **93**, 4965 (1990).
[107] T. J. Lee, A. Willetts, J. F. Gaw, and N. C. Handy, J. Chem. Phys. **90**, 4330 (1989).
[108] E. D. Simandiras, J. F. Gaw, and N. C. Handy, Chem. Phys. Lett. **141**, 166 (1987).
[109] J. F. Gaw and N. C. Handy, Chem. Phys. Lett. **128**, 182 (1986).
[110] W. Thiel, G. Scuseria, H. F. Schaefer III, and W. D. Allen, J. Chem. Phys. **89**, 4965 (1988).
[111] W. Thiel, Y. Yamaguchi, and H. F. Schaefer III, J. Mol. Spectrosc. **132**, 193 (1988).
[112] W. Schneider and W. Thiel, Chem. Phys. Lett. **157**, 367 (1989).
[113] H. Bürger, W. Schneider, S. Sommer, W. Thiel, and H. Willner, J. Chem. Phys. **95**, 5661 (1991).
[114] A. G. Császár, J. Phys. Chem. **96**, 7898 (1992).
[115] J. M. L. Martin, P. R. Taylor, and T. J. Lee, Chem. Phys. Lett. **205**, 535 (1993).
[116] J. M. L. Martin, T. J. Lee, and P. R. Taylor, J. Mol. Spectrosc. **160**, 105 (1993).
[117] J. M. L. Martin, T. J. Lee, and P. R. Taylor, J. Chem. Phys. **97**, 8361 (1992).
[118] J. M. L. Martin and T. J. Lee, Chem. Phys. Lett. **200**, 502 (1992).
[119] K. P. Huber and G. Herzberg, *Constants of Diatomic Molecules* (Van Nostrand, Princeton, NJ, 1979).
[120] Each F_{ijkl} constant was taken as the mean of the six estimators corresponding to all possible (ij,kl) combinations, regardless of any equivalences among the indices causing some of these estimators to not be unique. The RHF density matrix and CPHF convergence criteria in GAUSSIAN92 were both set to 10^{-12} in the second derivative computations.
[121] P. Pulay, in *Modern Theoretical Chemistry*, edited by H. F. Schaefer III (Plenum, New York, 1977), Vol. 4, p. 153.
[122] INTDER is a general program written by W. D. Allen which performs sundry vibrational analyses and higher-order nonlinear transformations among force field representations.
[123] Z. Cihla and J. Plíva, Coll. Czech. Chem. Commun. **28**, 1232 (1963).
[124] M. A. Pariseau, I. Suzuki, and J. Overend, J. Chem. Phys. **42**, 2335 (1965).

[125] Y. Morino, K. Kuchitsu, and S. Yamamoto, Spectrochim. Acta Part A **24**, 335 (1968).
[126] A. R. Hoy, I. M. Mills, and G. Strey, Mol. Phys. **24**, 1265 (1972).
[127] G. Fogarasi and A. G. Császár, Spectrochim. Acta Part A **44**, 1067 (1988).
[128] A. G. Császár and G. Fogarasi, Spectrochim. Acta Part A **45**, 845 (1989).
[129] A. G. Császár, G. Fogarasi, and J. E. Boggs, J. Phys. Chem. **93**, 7644 (1989).
[130] M. Vučelić, Y. Öhrn, and J. R. Sabin, J. Chem. Phys. **59**, 3003 (1973).
[131] J. Pacansky, U. Wahlgren, and P. S. Bagus, Theor. Chim. Acta **41**, 301 (1976).
[132] T. Ha, C. E. Blom, and H. H. Günthard, Chem. Phys. Lett. **70**, 473 (1980).
[133] See AIP document no. PAPS JCPSA-102-8506-5 for 5 pages of anharmonic vibrational data for deuterated ketenes. Order by PAPS number and journal reference from American Institute of Physics, Physics Auxiliary Publication Service, 500 Sunnyside Boulevard, Woodbury, NY 11797-2999. Fax: 516-576-2223, e-mail: janis@aip.org. The price is $1.50 for each microfiche (60 pages) or $5.00 for photocopies of up to 30 pages, and $0.15 for each additional page over 30 pages. Airmail additional. Make checks payable to the American Institute of Physics.
[134] W. D. Allen and H. F. Schaefer III, J. Chem. Phys. **89**, 329 (1988).
[135] A. Chédin, J. Mol. Spectrosc. **76**, 430 (1979).
[136] F. Hegelund, J. L. Duncan, and D. C. McKean, J. Mol. Spectrosc. **65**, 366 (1977).
[137] J. L. Duncan, D. C. McKean, and P. D. Mallinson, J. Mol. Spectrosc. **45**, 221 (1973).
[138] J. L. Teffo, O. N. Sulakshina, and V. I. Perevalov, J. Mol. Spectrosc. **156**, 48 (1992).
[139] R. D. Brown, P. D. Godfrey, and R. Champion, J. Mol. Spectrosc. **123**, 93 (1987).
[140] M. R. Aliev and J. K. G. Watson, J. Mol. Spectrosc. **61**, 29 (1976).
[141] J. Y. Beach and D. P. Stevenson, J. Chem. Phys. **6**, 75 (1938).
[142] D. Kivelson and E. B. Wilson, J. Chem. Phys. **20**, 1575 (1952).
[143] T. Oka and Y. Morino, J. Mol. Spectrosc. **6**, 472 (1961).
[144] J. Kraitchman, Am. J. Phys. **21**, 17 (1953).
[145] Modification of the Kraitchman relations for the case of a symmetric, multiple isotopic substitution is described by A. Chutjian, J. Mol. Spectrosc. **14**, 361 (1964).
[146] S. W. Staley, T. D. Norden, W. H. Taylor, and M. D. Harmony, J. Am. Chem. Soc. **109**, 7641 (1987).
[147] J. R. Thomas, B. J. DeLeeuw, G. Vacek, T. D. Crawford, Y. Yamaguchi, and H. F. Schaefer III, J. Chem. Phys. **99**, 403 (1993).
[148] C. W. Bauschlicher, Jr. and H. Partridge, J. Chem. Phys. **100**, 4329 (1994).
[149] A. G. Császár and W. D. Allen, J. Chem. Phys. (submitted).
[150] M. Lacy, Mol. Phys. **45**, 253 (1982).
[151] J. L. Duncan, Mol. Phys. **28**, 1177 (1974).
[152] R. D. Brown and R. G. Dittman, Chem. Phys. **83**, 77 (1984).
[153] P. R. Taylor, J. Comput. Chem. **5**, 589 (1984).
[154] F. Wang, M. A. Winnik, M. R. Peterson, and I. G. Csizmadia, J. Mol. Struct. (THEOCHEM) **232**, 203 (1991).
[155] J. P. Foster and F. Weinhold, J. Am. Chem. Soc. **102**, 7211 (1980).
[156] P. C. Hariharan and J. A. Pople, Theor. Chim. Acta **28**, 213 (1973).
[157] C. B. Moore and G. C. Pimentel, J. Chem. Phys. **40**, 329 (1964).
[158] P. v. R. Schleyer (personal communication). At the 6-31G** MP2 level of theory, the species $H_2A{=}CH_2$ exhibit θ_e(H–A–H) values of 116.9°, 121.2°, and 126.8°, respectively, for A=C, N^+, and O^{2+}. In this series the increase in θ_e appears to be a σ withdrawing effect arising from electronegativity differences.
[159] S. J. Klippenstein, A. L. L. East, and W. D. Allen, J. Chem. Phys. **101**, 9198 (1994).
[160] S. J. Klippenstein, A. L. L. East, and W. D. Allen, J. Chem. Phys. (submitted).